

Journal Pre-proofs

Proton Conducting Electrolytes Composed of Chondroitin Sulfate Polysaccharide and Citric Acid

Filipe M. Santos, Paula C. Barbosa, Rui F.P. Pereira, M. Manuela Silva, Helena M.R. Gonçalves, Sílvia C. Nunes, Filipe L. Figueiredo, Artur J.M. Valente, Verónica de Zea Bermudez

PII: S0014-3057(19)31905-6
DOI: <https://doi.org/10.1016/j.eurpolymj.2019.109453>
Reference: EPJ 109453

To appear in: *European Polymer Journal*

Received Date: 18 September 2019
Revised Date: 28 November 2019
Accepted Date: 12 December 2019

Please cite this article as: Santos, F.M., Barbosa, P.C., Pereira, R.F.P., Manuela Silva, M., Gonçalves, H.M.R., Nunes, S.C., Figueiredo, F.L., Valente, A.J.M., de Zea Bermudez, V., Proton Conducting Electrolytes Composed of Chondroitin Sulfate Polysaccharide and Citric Acid, *European Polymer Journal* (2019), doi: <https://doi.org/10.1016/j.eurpolymj.2019.109453>

This is a PDF file of an article that has undergone enhancements after acceptance, such as the addition of a cover page and metadata, and formatting for readability, but it is not yet the definitive version of record. This version will undergo additional copyediting, typesetting and review before it is published in its final form, but we are providing this version to give early visibility of the article. Please note that, during the production process, errors may be discovered which could affect the content, and all legal disclaimers that apply to the journal pertain.

© 2019 Published by Elsevier Ltd.



Proton Conducting Electrolytes Composed of Chondroitin Sulfate Polysaccharide and Citric Acid

Filipe M. Santos^{a,*}, Paula C. Barbosa^b, Rui F. P. Pereira^c, M. Manuela Silva^c, Helena M. R. Gonçalves^{a,d}, Sílvia C. Nunes^{e, f}, Filipe L. Figueiredo^b, Artur J. M. Valenteg, Verónica de Zea Bermudez^{a*}

^a Department of Chemistry/CQ-VR, University of Trás-os-Montes e Alto Douro, 5001-801 Vila Real, Portugal;

^b Department of Materials and Ceramic Engineering/ CICECO – Aveiro Institute of Materials, University of Aveiro, 3810-193 Aveiro, Portugal;

^c Chemistry Center and Chemistry Department, University of Minho, 4710-057 Braga, Portugal;

^d REQUIMTE, Instituto Superior de Engenharia do Porto, 4200-072 Porto, Portugal;

^e Chemistry Department, University of Beira Interior, 6201-001 Covilhã, Portugal;

^f Department of Chemistry, University of Trás-os-Montes e Alto Douro, 5001-801 Vila Real,

^g Chemistry Department, University of Coimbra, Coimbra, Portugal;

* Correspondence: filipems@utad.pt (F.M.S); vbermude@utad.pt (V.d.Z.B.); Tel.: +351-259-350000 (V.d.Z.B.)

Abstract: Novel electrolytes composed of chondroitin sulfate A (CSA) and citric acid (CA) have been prepared using a clean, safe, and fast route. These electrolytes exhibit different physical-chemical properties, depending on the amount of CA. For $X > 82.3\%$, where X is the mass ratio, in %, of $CA/(CA+CSA)$, whitish polycrystalline powders result. Lower amounts of CA leads to the production of translucent, amorphous films, sticky for $X = 75.6$ and 82.0 , brittle for $X < 43.6$ and crack-free, self-standing for $43.6 < X < 75.6$ %. The results obtained provide evidence that, at low pH, strong hydrogen bonding interactions take place between the anionic sulfonic and carboxylic groups of CSA and CA. CA exerts a key role, acting as a cross-linker and proton source, while simultaneously influencing sample morphology. At room temperature the highest ionic conductivity is achieved at $X = 60.8$ %. A significant enhancement of the ionic conductivity of this sample occurs with the increase of relative humidity (RH) (from 3.1×10^{-7} to 3.7×10^{-2} S cm^{-1} 30% for RH = 30 and ~100%, respectively).

Keywords: chondroitin sulfate; biopolymer electrolytes; ionic conductivity; citric acid;

Declarations of interest: None

1. Introduction

According to the United Nations (UN), environmental and energy issues are two of the major challenges human society has to face. These problems have become so complex and taken on a global scale that, for the last decades, a call for game-changing technology that can lead to sustained development has consistently been issued [1]. In its latest iteration of the global sustainable development agenda, the UN has adopted 17 goals intended to prompt action from human agents in areas of critical importance for the sustained development of both human society and the planet [2]. Energy-wise, the UN goal aims to “ensure access to affordable, reliable, sustainable and modern energy for all” by focusing on three main areas: energy efficiency, renewable energy and energy access [2]. Access to reliable and sustainable energy sources has prompted the development of new technologies capable of addressing both the human need for energy as well as minimize the ecological consequences associated with its use. In this sense, the choice for chemistries that can minimize the ecological footprint and / or are easily integrated in a full circular economy needs to be prioritized.

In this context, biorenewable natural products, such as polysaccharides and proteins, are increasingly being held as ideal materials for the production of solid polymer electrolytes (SPEs), both from an economic and an environmental point of view [3-5]. The interest in SPEs [6,7] has been steadily increasing, due to their applications in various solid state electrochemical devices, such as batteries, sensors, fuel cells, solar cells and electrochromic devices [8–11].

Polysaccharides are a versatile and rich family of macromolecules whose structure and thermodynamics have been extensively investigated. Polysaccharides comprise some of the most abundant biopolymers on Earth [5,12]. Polysaccharides, such as starch, heparin, cellulose, chitosan, hyaluronic acid or agar, among others, have been blended, doped, combined or otherwise manipulated with suitable substrates to produce ion conducting materials [12-19]. A popular strategy for the production of novel SPEs based on polysaccharide host polymers is to dope them with ionic liquids (ILs). The underlying objective is the combination of the polysaccharides' properties with other desirable properties present in the ILs, namely their high thermal stability, wide electrochemical potential window, moderate viscosity, good redox stability, plasticizing and lubricating properties [13,14,20]. However, ILs have been found to possess some disadvantages: (1) they may be more toxic than first expected [21-23] and (2) IL leakage problems have been reported [24]. These drawbacks motivated the development of another type of materials with physical properties and phase behavior similar to those of ILs. These materials, classed as deep eutectic solvents (DESs), possess a melting point lower than those of their individual constituents and low enough to be used as solvents. Because they are synthesized from eutectic mixtures of Lewis/Brønsted acids and bases derived from natural sources (e.g., aminoacids, carboxylic acids, sugars, urea and choline), DESs are economically cheaper and environmentally friendlier than conventional ILs [25-29].

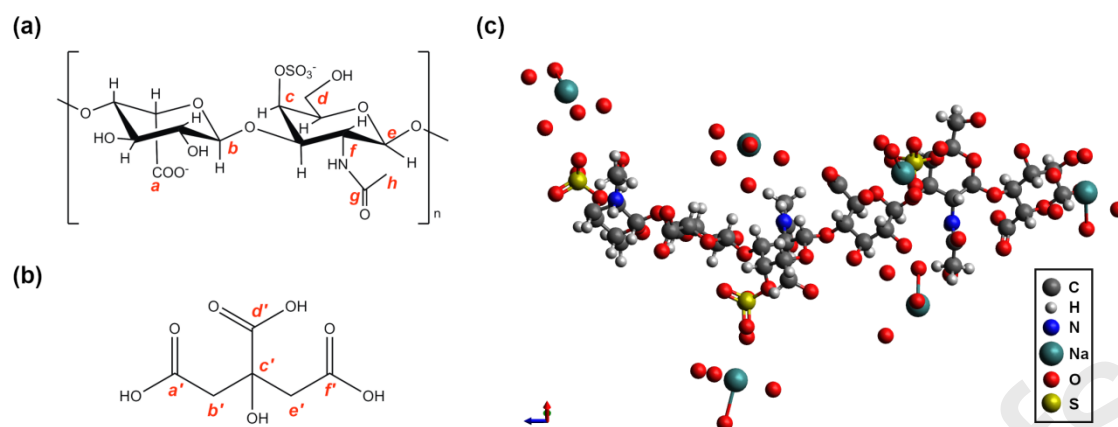


Figure 1. Representation of the chemical structure of the disaccharide unit of CSA (a), a form of chondroitin sulfate, of citric acid (b), and of the asymmetric unit of the sodium salt of CSA (c), which was used in this work, as obtained from the data collected from [30].

Following our previous works on polysaccharide-based electrolytes [13,14,31], we turned our attention to chondroitin sulfate (CS) as a potential SPE due to its anionic character and benign nature. CS is a naturally occurring linear polysaccharide (Figure 1a) that is particularly abundant in the connective tissue of mammals, but also in invertebrates and even some bacteria. Similarly to what is found in the case of other biopolymers extracted from living organisms, CS chains exhibit significant structural variation in terms of molecular mass, arrangement of disaccharide units, sulfation pattern and charge density, among others [32,33]. However, all forms of CS share common structural features, including assemblages of disaccharide units mainly composed of $\beta(1,4)$ -*D*-glucuronic acid and $\beta(1,3)$ -*N*-acetyl-*D*-galactosamine, incorporating hydroxyl, amide and carboxyl groups, and held together by glycosidic linkages (Figure 1a) [32,33]. Sulfonic groups are often attached in either the C-4 or C-6

positions of the galactosamine residue. These two forms of CS are usually known as CSA and CSC, respectively. Other disaccharide sulfation patterns have also been reported which differ in terms of number (ranging from non-sulfated disaccharide units to disulfated disaccharides) or position (the second sulfonic group appearing in either the galactosamine residue or the glucuronic acid moiety). CS is known to be highly stable, hydrophilic, easily chemically modified, and exhibits low toxicity and good biodegradability [34]. Furthermore, electrolyte complexes can be formed with inorganic acids [35], metal cations [35] and cationic biopolymers, such as chitosan [36–40]. Curiously, until now research conducted with this polyanion has been mostly restricted to therapeutic applications, such as tissue engineering [34,41,42] and drug delivery [39,41,43].

Inspired by the DES concept, we combined CSA with citric acid (CA) (Figure 1b), an organic polyprotic acid naturally occurring in citrus fruits. CA is known for its ability to establish hydrogen bonds [44] and form low-temperature transition mixtures (i.e. DESs) with other organic entities, namely choline, various sugars or proline [30,45]. Also of note is the increasing use of CA as a plasticizer [46,47] and a cross-linker [44,46], including in the preparation of proton exchange membranes [47]. A similar strategy was employed in the preparation of SPEs composed of chitosan and carboxylic acids, such as oxalic acid [48,49], acetic acid [50] or maleic acid [16]. It is necessary to highlight that CSA has remained practically unexplored as a promising host polymer candidate for SPEs, in spite of the significant presence of sulfonic groups. Interestingly, just one work on the proton conductivity of a composite prepared from CSA, chitosan and

hydroxyapatite was found in the literature [51]. The proton conductivity values registered by this composite are higher than that reported for Nafion [51].

The SPEs here described were synthesized by means of a clean, safe and cheap procedure, and their structure, thermal and electrochemical properties were investigated. These electrolytes, henceforth noted as CA:CSA(X), where X is the mass ratio, in %, of CA/(CA+CSA) ($15.2 \leq X \leq 93.7$).

2. Materials and Methods

2.1. Reagents and synthetic procedures

Chondroitin sulfate A, sodium salt (CSA, 90% pure, Alfa Aesar lot.: 61301303), and anhydrous citric acid (CA, 99.5+% pure, grade ACS, ISO. Reag. Ph. Eur, Merck, Inc) were used as received. Distilled water was used throughout in all experiments.

In a typical experiment, a solution of CA (3.00 g/6.00 mL H₂O) was added to an aqueous solution of CSA (4% wt.) and stirred for about 10 min. Different amounts of CA were added, ranging from 0.12 to 6 mL, depending on the specific mass ratio of CSA/CA intended. In all cases, the total volume varied from 9 to 11 mL, depending on the specific CSA/CA ratio used (Table S1 in the Supplementary Materials). The pH of the solution was checked before and after CA addition, and the resulting solution was carefully poured onto custom-made Teflon molds (5-cm inner diameter a rough surface

due to use) and allowed to dry. After a drying period of 4-5 days during which the solution was left to evaporate in air, the resulting materials were collected and analyzed.

2.2. Methods

Fourier transformed infrared spectra obtained in attenuated total reflectance mode (ATR-FTIR) spectra were recorded with an IRAffinity-1S Shimadzu spectrometer equipped with a horizontal unique reflection ATR accessory (Golden Gate). The sample was placed over the diamond crystal with the help of a spatula. All spectra were obtained with 128 scans between 4000 and 400 cm^{-1} with a resolution of 2 cm^{-1} .

The differential scanning calorimetry (DSC) curves of the samples were recorded at a heating rate of 10 $^{\circ}\text{C min}^{-1}$ under a flowing argon atmosphere. Each sample was placed in a 40 μL perforated aluminum pan and the thermogram was recorded using a Mettler DSC 821e.

Thermogravimetric analyses (TGA) and additional DSC measurements were carried out in a DTA/TGA Netsch STA 449F3 thermal analyzer. In a typical experiment, samples were heated from room temperature to 700 $^{\circ}\text{C}$ in alumina (Al_2O_3) crucibles under a nitrogen (N_2) atmosphere (50 mL min^{-1} purge; 20 mL min^{-1} protective flow), with a heating rate of 10 $^{\circ}\text{C min}^{-1}$.

Polarized optical microscopy (POM) images were recorded in an OPTIKA B-600 Pol microscope. The images were obtained through a digital camera 8 Mpixel Digital Photo and were analyzed with Optika Vision Pro software.

Solid state nuclear magnetic resonance (NMR) experiments were conducted at CICECO – Aveiro Materials Institute, using a Spectrometer Bruker Avance III 400 wide-bore (400 MHz, ^1H Larmor frequency). A 4 mm double-resonance magic angle spinning (MAS) probe was employed at 100.6 MHz (^{13}C) Larmor frequency. Samples were spun in ZrO_2 rotors using a spinning rate of 12 kHz. ^{13}C cross polarizational (CP)/MAS NMR spectra were recorded using a ramp step (varying from 100 to 50% in amplitude using 100 points), with a recycle delay of 5 s, a contact time of 2.0 ms and ^1H 90° excitation pulse of 3.20 μs . All chemical shifts are quoted in parts per million (ppm) from tetramethylsilane (TMS).

pH measurements were obtained with a HANNA pH20 pH-meter at room temperature. All buffer solutions employed in the calibration of the pH-meter were obtained from VWR Chemicals.

The ionic conductivity (σ) of the samples was determined under real conditions by locating an electrolyte disk between two 10 mm diameter ion-blocking gold electrodes (Goodfellow, >99.95%) to form a symmetrical cell. The electrode/sample/electrode assembly was secured in a suitable constant volume support and installed in a Büchi TO51 tube oven with a K-type thermocouple placed close to the electrolyte disk to measure the sample temperature. Bulk conductivities of the samples were obtained during heating cycles by using the complex plane impedance technique with the Autolab PGSTAT-12 (Eco Chemie) equipment between room temperature and 110 $^\circ\text{C}$ and at approximately 15 $^\circ\text{C}$ intervals. The ambient relative humidity (RH) was lower than 30%.

The ionic conductivity of membranes was also determined at room temperature (~26 °C) and under variable RH (30-98%) by impedance spectroscopy using an Agilent E4980A Precision LCR meter. The through-plane (TP) configuration was adopted and the membranes were placed between two carbon cloth gas diffusion layers (~0.5 cm²) and graphite plates with gas channels. The samples were mounted on an appropriate support and placed in a climatic chamber made in-house, where variable relative humidity (RH) conditions were achieved using different saturated salts solutions. The RH was constantly monitored close to the sample with a humidity sensor. The impedance spectra were collected between 20 Hz and 2 MHz with a test signal amplitude of 100 mV. Spectra were analyzed with ZView (Version 2.6b, Scribner Associates) to assess the ohmic resistance (R), which was normalized to the samples geometry to calculate the conductivity through the usual formula $\sigma = L(RA)^{-1}$, where L is the distance between the in-plane silver stripes (or the thickness of the membranes) and A is the cross-section area of the membranes (or the surface area of the electrodes).

The Atomic Force Microscopy (AFM) analysis was performed in an AFM CSI Nano-Observer equipment (Scientec) in tapping mode using a super sharp Si HQ:NSC19/FORTA probe with a frequency resonance of 60 kHz and a spring constant of 0.3 N m⁻¹. In order to improve the quality of the images, a flattening and elimination of line noise tools were applied using the Gwyddion 2.52 software. Because the samples produced were dried in air, the surface of the film was exposed to N₂ prior to AFM analysis to clean any dust and fibers that might have been trapped due to air exposure. As the film was rather sticky, additional precautions were undertaken to

avoid the insertion of indentations or film stretching. The film was deposited on double tape glue that was previously homogenized on the support to avoid the formation of bubbles. The AFM analysis was performed on the surface which had been exposed to air during the drying process. Indeed, due to the nature of the film itself, the surface in contact with the mold mimicked its patterns (e.g., scratches caused by prolonged use, including removal of films with spatula) (Figure S1 in the Supplementary Material). Therefore it was decided that the analysis of the surface exposed to air would provide a deeper knowledge of the topographical characteristics of the film, regardless of the mold used.

Scanning electron microscopy (SEM) images of the top (exposed to air during drying) and bottom (in contact with the Teflon mold) surfaces, as well as the cross-section, of the samples were obtained at 20 kV on a Hitachi S-3400N type II microscope (Hitachi, Chiyoda, Japan) equipped with a Bruker x-flash 5010 at high vacuum. For the cross-section analyses, the cut was made at cryo-temperatures. All the samples were coated with gold in a rotating holder to ensure homogeneous distribution. Elemental mapping of the samples was performed by energy dispersive spectroscopy (EDS) X-ray analysis. The acceleration voltage and intensity of the beam current were chosen taking into consideration the chemical composition of the samples. In addition, both parameters were optimized to maximize high count and low deadtime. The acquisition time for a satisfactory resolution and noise performance was 60 s. As the films were flat, the directionality was neglected in the measurements.

3. Results and Discussion

CSs are low charge density structures which include several functional groups prone to protonation (Figure 1a): most notably an amide group, a carboxylic group and a sulfonic group, but also an ether and hydroxyl groups, meaning that the same structure features both weak and strong acidic groups [32,37]. In our working conditions, the measured pH of a 4% aqueous solution of CSA was 6.0, indicating that both the weakly acidic carboxylic group (pKa 3.5-4.6) and the strongly acidic sulfonic group (pKa 2.6) were deprotonated [32,52].

Table 1. Relevant data of the synthesis of the CA:CSA(X) electrolytes.

X (%)	pH	Product	H ₂ O content (wt/wt %)*
0	6.03	brittle film	11.41
15.2	3.55	brittle film	09.53
29.2	3.12		10.01
43.6	2.89	flexible film	09.53
60.8	2.55		07.11
75.6	2.21	flexible, sticky film	06.67
82.3	2.07		07.43
83.4	2.00	Polycrystalline powders	06.91
84.4	1.95		07.48
86.1	1.88		04.54
90.3	1.73		06.18
92.5	1.66		06.77
93.7	1.62		07.86
100	1.42		

* - as measured by thermogravimetric analysis

The addition of a concentrated CA solution to the CSA aqueous solution led to an immediate drop in pH, and the concomitant appearance of some turbidity. However, this turbidity ultimately disappeared (Tables 1 and S1 in the Supplementary Material). Different combination mass ratios of CSA and CA, henceforth designated by CA:CSA(X) where X indicates the specific mass ratio used, afforded different end products, from powders to films (Table 1).

Films were obtained for a wide range of X values, ranging from 15.2 to 82.3%, from solutions with pH values as low as ~2.1 (Table 1 and Figure S2 in the Supplementary Material). These films exhibited different properties, depending on CA concentration. Thus, low concentrations of CA ($X < 43.6$ and $\text{pH} > 3.0$) afforded brittle films, probably due to the insufficient protonation of CSA by CA ($\text{p}K_{a1} = 3.13$, $\text{p}K_{a2} = 4.76$ and $\text{p}K_{a3} = 6.40$) [53]. For $43.6 < X < 70.1$ ($2.55 < \text{pH} < 2.89$) non sticky films were produced. Sticky flexible films were obtained for $70.1 < X < 82.3$ ($2.07 < \text{pH} < 2.29$). These results point out a trend between the flexibility of the film and the increasing amount of CA, as a result of the formation of new intermolecular hydrogen bonds which occurs at the expense of the existing intramolecular interactions of CSA [54]. Moreover, this trend confirms the CA role as a plasticizer in the formation of SPEs [46,47].

The incorporation of higher amounts of CA ($X > 83.4\%$, $\text{pH} \leq 2.0$) led to the gradual precipitation of a white powder. Given the observed pH of the parent solution, a strong interaction between the CA and the anionic polysaccharide was expected, in a similar manner as reported for other SPEs obtained with CSA at low pH [55].

3.1. Spectroscopic Characterization of the CA:CSA Electrolytes

3.1.1. ^{13}C CP-MAS NMR spectroscopy

^{13}C NMR spectroscopy is known to provide relevant information about the structure of CSA and related polysaccharides, such as the pattern of sulfation, conformation of the polysaccharide or even hydrogen bonding [56,57]. The ^{13}C CP-MAS NMR data collected for both the starting materials are presented and discussed in the Supplementary material.

The ^{13}C CP/MAS NMR spectra of the CA:CSA electrolytes exhibit signals pertaining to both CSA and CA (Figure 2 and Figures S3, S4 and Table S2, Supplementary Material). At $X = 60.8$ the ^{13}C CP/MAS NMR spectrum is still dominated by the CSA resonances. However, the carboxyl resonance, centered at 176.0 ppm, appears as a broad, asymmetric signal, with new shoulders at 179.4 and 173.6 ppm due to the carboxylic groups present in the CA moiety (Figure 2). A new broad signal located at 43.7 ppm emerges, due to the CA methylene carbons (Figure S3). As higher amounts of CA are progressively added to the CSA biopolymer, several changes occur until the spectra are entirely dominated by the characteristic resonances of CA (at $X \geq 82.3$). The sharpening of the signals seen for $X \geq 82.3$, indicate the high structural order of the powdered material, in contrast with the broad signals produced by films (for $X < 82.3$).

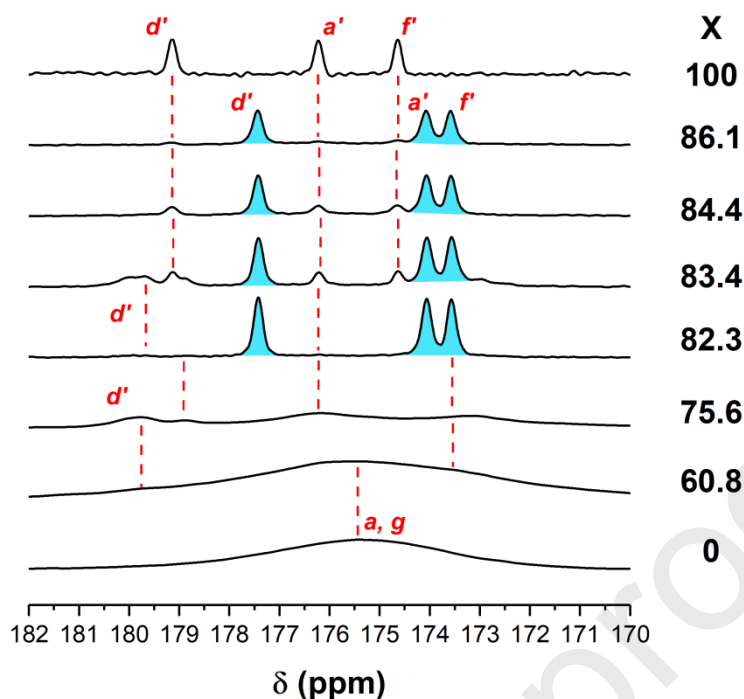


Figure 2. ^{13}C CP-MAS NMR expansion for the carbonyl carbon groups of CSA, CA and the various electrolytes prepared. Blue shaded peaks are due to CA monohydrate.

Two different regions are of particular interest: the region between 182 and 170 ppm (Figure 2), corresponding to the carbonyl groups, and the region between 110 and 90 ppm, related to the glycosidic bonding (Figure S4).

In the carbonyl region ($182 < \text{ppm} < 170$), the CSA signal at 176 ppm is visible up to $X = 60.8\%$, with higher amounts of added CA leading to spectra dominated by the resonances of the CA carboxylic groups (Figure 2). In the spectra of CA:CSA electrolytes with $82.3 \leq X < 100$, three prominent resonances are observed at 177.4, 174.1 and 173.6 ppm, which do not coincide with the characteristic resonances of the CA precursor, observed at 179.4, 176.0 and 174.6 ppm (Figure 2). Fisher *et al.* have associated those resonances with CA monohydrate [58]. In addition, weak signals at 179.2, 176.2 and

174.6 ppm are seen in some spectra, indicating the presence of a secondary phase consisting of anhydrous CA, as suggested by the spectrum of the pure precursor and by the literature data [58]. As the ^{13}C CP/MAS NMR spectra for the CA:CSA electrolytes with $X > 82.3$ are dominated by the resonances of CA in its various forms, we can conclude that for these particular formulations, there is an excess of CA present in the collected powders. In $X > 82.3$, the predominance of the CA monohydrate signals over the CA anhydrous signals strongly suggests that the powders here obtained are mostly constituted by CA monohydrate with a secondary phase consisting of CA:CSA(X) electrolytes, which could be justified by the considerable CA molecular aggregation arising from the hydrogen bonding interaction between both CA and water [59].

Over the whole X range investigated, no signals above 180 ppm were detected. The absence of these signals, which are related with the formation of sodium citrate [58], indicates that the sodium counter-ions present in the raw CSA sample did not complex with CA.

In the region between 110 and 90 ppm (Figure S4), the broad signal observed at 102.8 ppm, for CSA, gradually shifted into a duplet at $X = 75.6$, as a consequence of a change in the chemical environment of the glycosidic bridge [60,61]. According to previous works [60–62], two resonances are expected in this region of the CSA ^{13}C NMR spectrum, respectively at 106.5–105 and 103.5–102 ppm, due to the (1–4)- β -linked C-1 carbon (peak *b*) and (1–3)- β -linked C-1 carbon (peak *e*), respectively. In this work, the same resonances appear at 104.2 and 101.2 ppm. The envelope that contains both signals remains centered in the same area as the starting CSA material (Figure S3 and Table S2).

Hamer *et al.* observed no significant shift of these signals when CSA was acidified to a pH ~1. [60]. In a study involving the interaction between chondroitin sulfate-6 (CSC) and chitosan, the authors observed a shift of the resonance associated with the anomeric carbon from 104.7 to 99.3 ppm, which was attributed to the electrostatic interactions between both electrolytes [38]. Given that the difference between CSC and the CSA used in this work is simply the location of the sulfonic group (which in our case is located at the C4 position of the *N*-acetylgalactosamide ring, instead of the C6 position of the same ring), this might have led to a smaller upfield shift than that observed by Chen *et al.* [38], since the presence of sulfonic groups in neighboring atoms is known to induce higher chemical shifts [57].

From the gathered evidence, the nature of the interaction between CSA and CA is probably electrostatic, as observed for other materials containing CSA [37,38,63,64], especially at low pH (≤ 2). It has been argued that at low pH, a competition exists between the protonation of the polyanionic sites of CSA and their complexation with the Na^+ cations [37,38], which might result in the condensation of the acidic and sodium cations around the CSA backbone [65,66].

3.1.2. ATR-FTIR spectroscopy

The ATR-FTIR spectra of the CA:CSA electrolytes, and of pure CSA and CA are reproduced in Figures 3 and S5 (in the Supplementary Material). Relevant ATR-FTIR data are collected in Table S3. Of particular interest is the spectral interval of 1800-600

cm^{-1} , found to be the most useful for the identification of the vibrational modes of CSA and CA [67,68].

The analysis of these ATR-FTIR spectra is complicated by the fact that vibrational modes of different origins appear superimposed in most of the spectral regions.

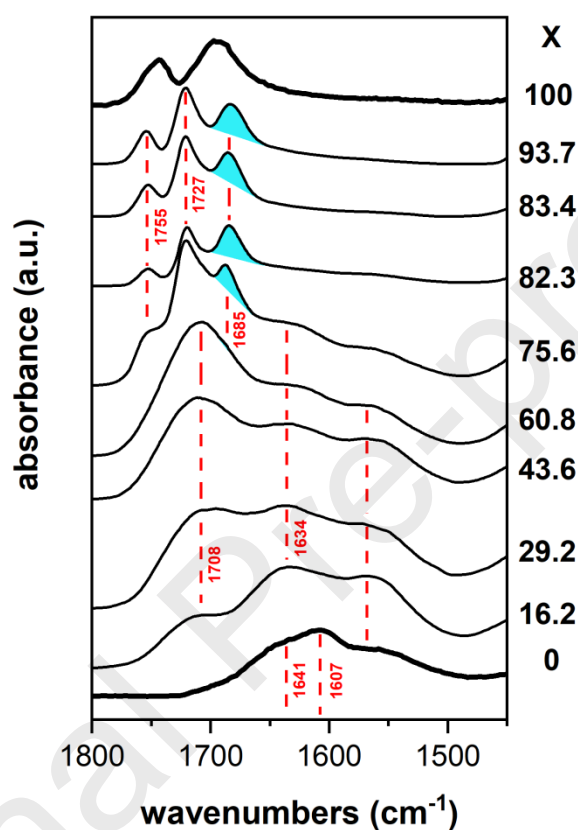


Figure 3. ATR-FTIR spectra of CSA, CA and selected CA:CSA(X) electrolytes in the 1800-1450 cm^{-1} region. Blue shaded bands indicate the presence of CA monohydrate.

In the spectrum of CSA, the asymmetric stretching vibration of the carboxylate groups ($\nu_{\text{as}}\text{COO}^-$) emerges as a very strong band centered at 1607 cm^{-1} with two shoulders at 1641 and 1551 cm^{-1} (Figure 3), due to the Amide I and Amide II vibrations, respectively [68–72]. According to the literature, the shift of the CSA band at 1611 cm^{-1}

to lower wavenumbers (1607 cm^{-1}) is indicative of the presence of hydration waters, interacting with the carboxylate groups through hydrogen bonds [72].

The asymmetric stretching vibration of the carboxylic groups ($\nu_{\text{as}}\text{COOH}$) in CSA is expected between $1740\text{-}1720\text{ cm}^{-1}$ [37,69,71]. In the ATR-FTIR spectrum of CA the $\nu_{\text{as}}\text{COOH}$ mode is observed at 1743 and 1693 cm^{-1} (Figure 3). These bands are assigned to the central carboxylic group and to the terminal carboxylic groups, respectively [73–75].

When CSA and CA are combined, changes in the shape, number and wavenumber of the carboxylate bands can be seen in this particular region of the spectra, indicating strong interactions between both starting materials. As expected, as the amount of CA added to the CSA solution increased, the maximum of the band envelope due to the asymmetric stretching vibration of the carboxylate groups, $\nu_{\text{as}}\text{COO}^-$, mode of the polymeric moiety gradually shifted to higher wavenumbers, first with a band centered at 1708 cm^{-1} (for $X \leq 60.8$) and then with a band located at $\sim 1727\text{ cm}^{-1}$ (for $X \geq 75.6$) (Figure 3). This shift, along with the disappearance of the $\nu_{\text{as}}\text{COO}^-$ band at 1607 cm^{-1} is indicative of the gradual protonation of the electrolyte. At $X \geq 75.6$, two new bands are clearly seen at 1755 and $\sim 1685\text{ cm}^{-1}$ (Figure 3). The band located at 1685 cm^{-1} is attributed to the CA monohydrate [74]. The band at 1755 cm^{-1} is due to the presence of the dimeric form of CA [44,75], probably due to the establishment of hydrogen bonds between the carboxylic groups of each monomer [44,75]. The presence of this particular form of CA is only to be expected, given the low working pH (which favors hydrogen bonding) and is in agreement with the ^{13}C CP/MAS NMR data.

The symmetric stretching vibration of the carboxylate groups ($\nu_s\text{COO}^-$) [68–70,72–75] is located at 1408 cm^{-1} in CSA, 1416 cm^{-1} in CA and $1416\text{--}1419\text{ cm}^{-1}$ in the prepared CA:CSA adducts (Figure S5, Supplementary Material). No relevant changes were detected as a function of X.

Sulfonic characteristic modes [68–70,72] are found at 1224 cm^{-1} (with a shoulder at 1261 cm^{-1}), associated with the asymmetric stretching vibration of the sulfate groups $\nu_{\text{as}}(\text{OSO}_3^-)$ mode, and at 851 and 720 cm^{-1} , due to the asymmetric stretching vibration of the carbon-sulfate bond, $\nu_{\text{as}}(\text{C-O-S})$ (Figure S4). While the bands derived from the CSA carbon backbone remain unchanged in all the CA:CSA samples prepared, a shift of -18 cm^{-1} (from 1224 to 1206 cm^{-1}) was observed (Figure S5) in the $\nu_{\text{as}}(\text{OSO}_3^-)$ band as the amount of CA increased. Servaty *et al.* argued that the occurrence of the shoulder located at 1261 cm^{-1} might be due to non-symmetric water-mediated interactions between the Na^+ counterions and the sulfonic group [72]. As increasing amounts of CA were added to the CSA solution, the overall pH of the solution decreased. The pH thus approached the pK_a for $-\text{OSO}_3\text{H}$ (about 2.6), $[-\text{OSO}_3\text{H}] \approx [-\text{OSO}_3^-]$ and changes in the local chemical environment around the sulfonic groups occurred.

3.2. Morphological studies of the prepared electrolytes

As reported earlier, the combination of CSA and CA led to the formation of powders and films, depending on the value of X. Given that these two series of materials have very different properties, the discussion that follows henceforth will be focused exclusively on the films. The results obtained for the powders are reported in

the supplementary material. Films were formed at room temperature in a period of 4-5 days, following the addition of a concentrated CA solution to a 4% aqueous CSA solution. These translucent films were produced for all combinations of CSA and CA where $X < 82.3\%$ (Table 1).

The POM images confirm that CSA is practically amorphous (Figure 4A and 4B). However, when CA was added to the solution, isolated birefringent entities emerged in all the films, indicating the presence of crystalline regions (Figures 4C to 4H).

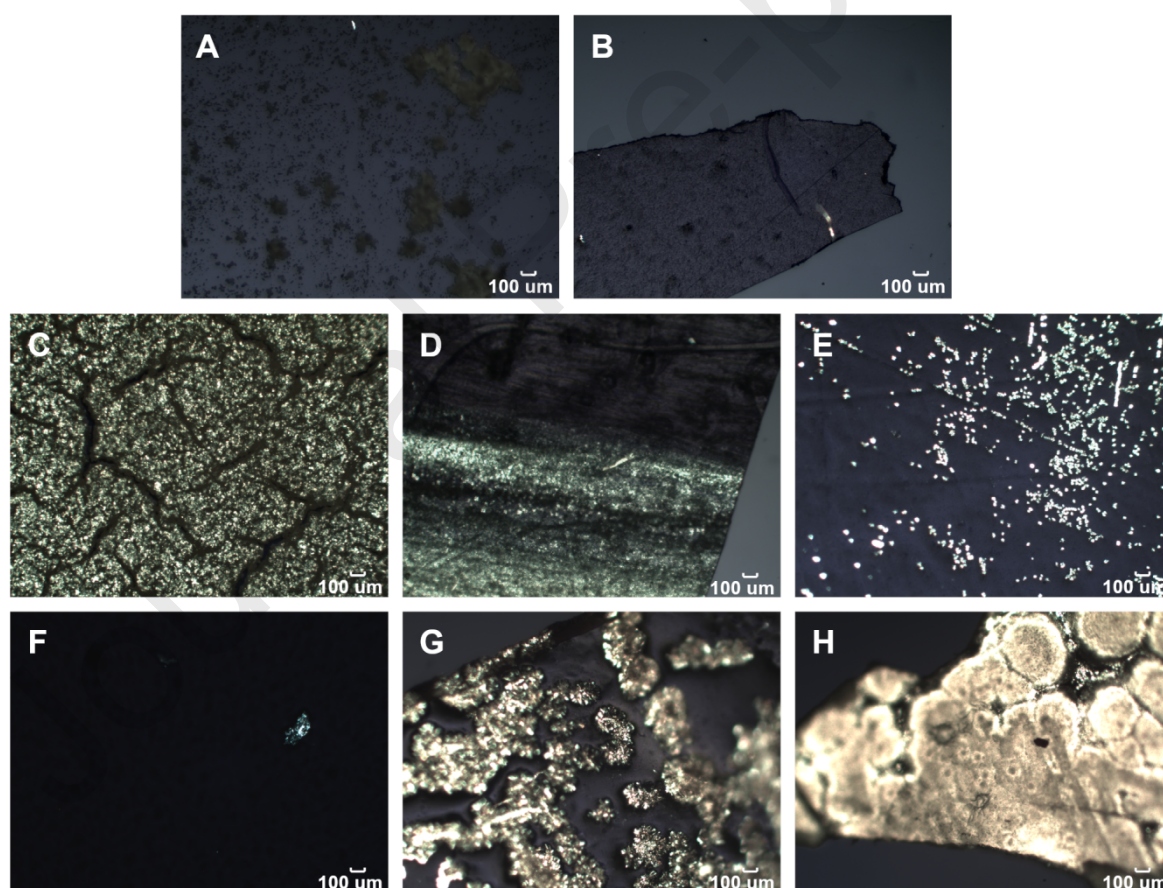


Figure 4. POM images obtained with crossed polarizers for CSA as received (A); CSA film (B); and CA:CSA(X) electrolytes with $X = 15.2$ (C); 29.2 (D); 43.6 (E); 60.8 (F); 75.6 (G) and 82.3 (H).

The SEM images of the top and bottom surfaces, as well as the cross section of films with $X < 60.8$ are represented in Figure 5. The smoothest surfaces were obtained for the CA:CSA(X) samples with $X = 60.8$ (Figure 5D) and 43.6 (Figure 5C). At higher X , the surfaces became more irregular, culminating with clearly visible cracks in $X = 82.3$ (Figure S6 in the Supplementary Material).

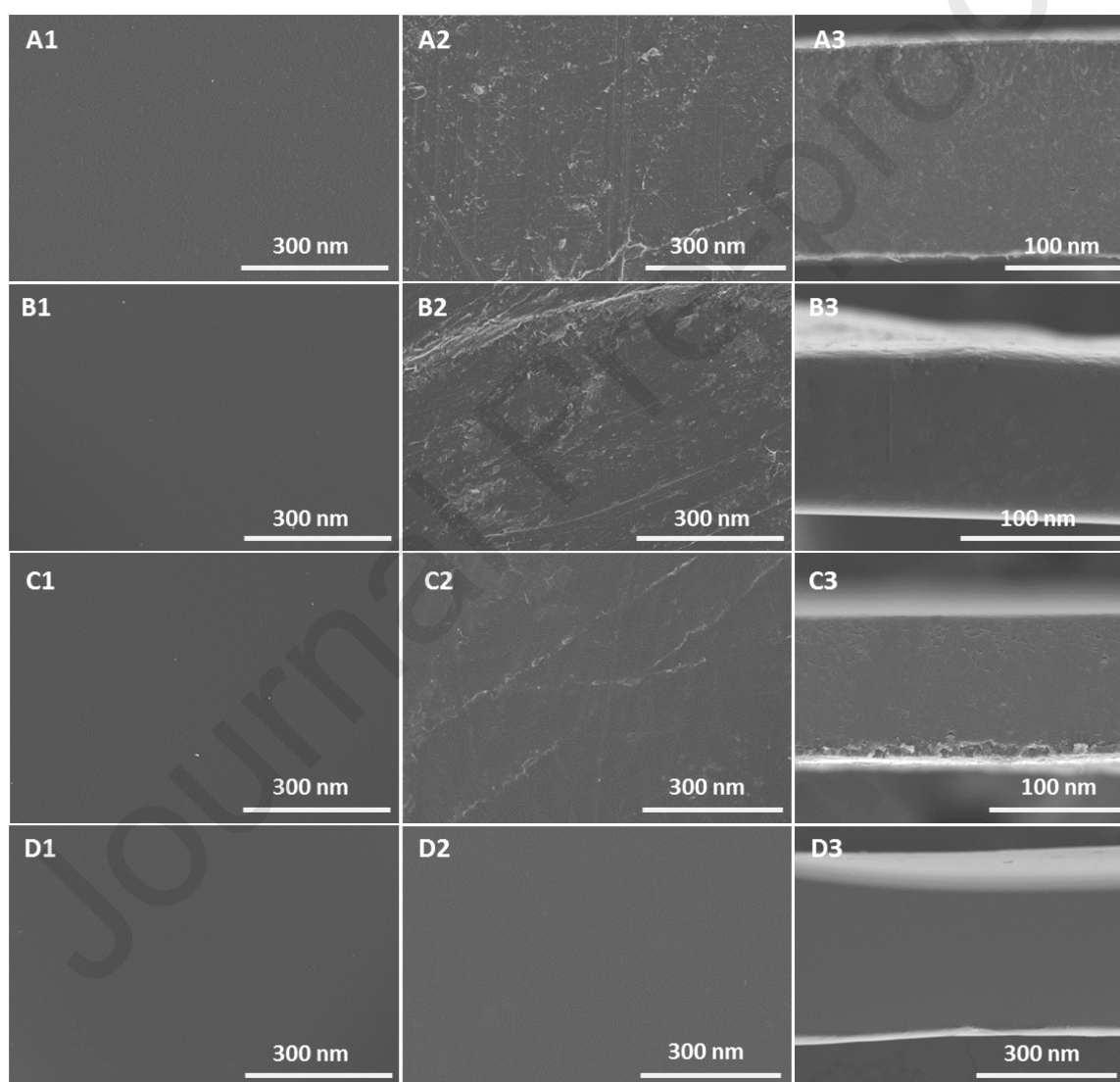


Figure 5. SEM images of the top (1) and bottom (2) surface, and cryogenic temperature cross-section (3) of the CA:CSA(X) films, with $X =$ (A) 15.2; (B) 29.2; (C) 43.6; and (D) 60.8.

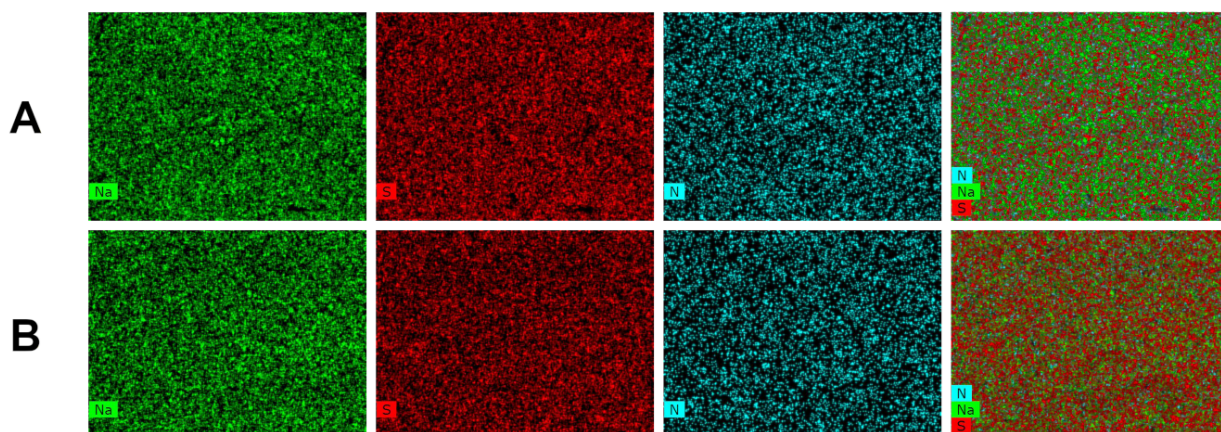


Figure 6. EDS mapping images for the top surfaces of the CA:CSA(X) films, with $X = 43.6$ (A); 60.8 (B) for the elements Na (green), S (red) and N (cyan). The last column is a composite image obtained from the juxtaposition of all three elements.

The corresponding EDSs mapping images for CA:CSA(X) films with $X = 43.6$ and 60.8 are shown in Figure 6. The distribution maps for the more concentrated films can be seen in Figure S7 in the Supplementary Materials. The obtained profiles for the distribution of S and N atoms (present only in CSA) demonstrate that the polymer is homogeneously distributed in the analyzed area. Moreover, for these films, the profile for the Na^+ cations matches that seen for the sulfonic group, suggesting that for CA-poor films where $X \leq 60.8$, the sulfonic groups are bound to the Na^+ cations.

The full scale view of the film placed on the AFM analysis support shows that the sample CSA/CA(60.8) is homogenous (Figure 7E) and the film topographical analysis revealed a medium roughness of 2.99 nm , which is consistent with the film macroscopic appearance. A close analysis revealed pore-like structures of different sizes and with a medium depth of 50 nm throughout the film (Figure 7A-D). Moreover, it is also possible

to see non-uniform structures (bright angular structures on the topographical images) that seem to have developed as the film dried out, since they are in different planes. These structures did not suffer any detectable morphology alteration by the action of the cantilever passage and their size range from 0.88 to 2.60 μm in length. Taking into consideration the film formation and the characteristics showed by AFM analysis, it is quite possible that these angular structures are indeed crystallites formed during the solvent evaporation process, as previously described by [59].

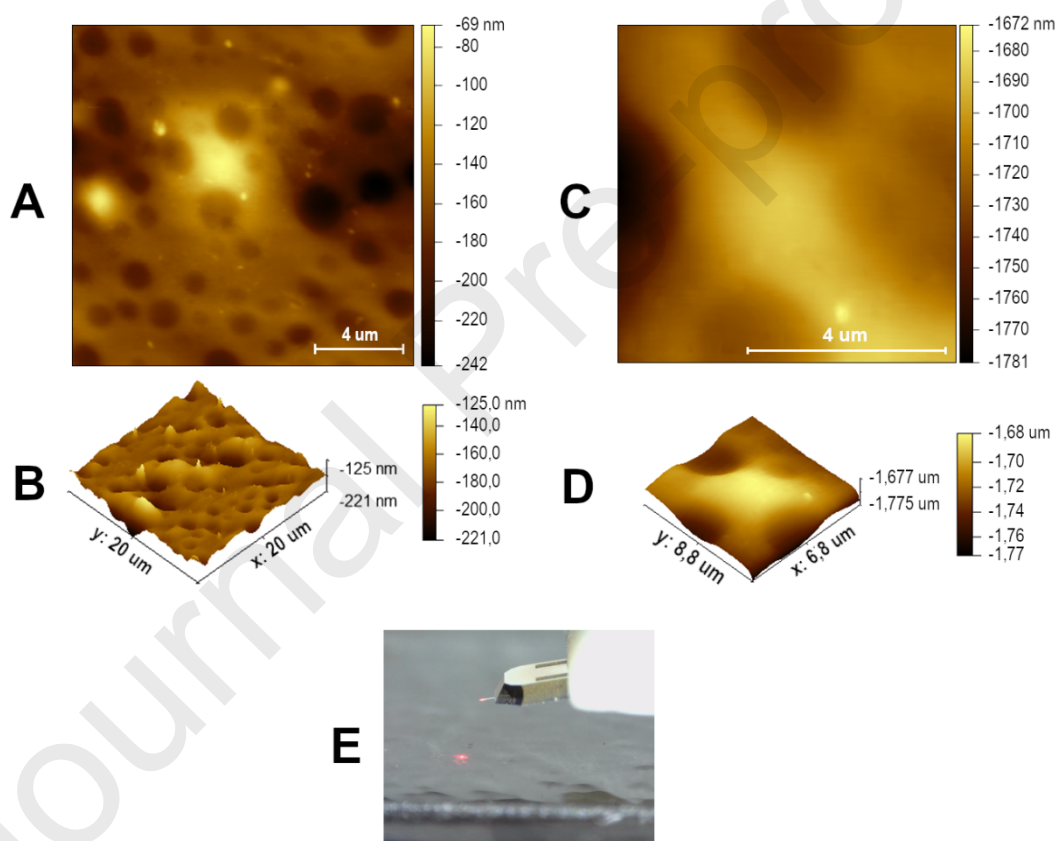


Figure 7. AFM characterization of the CA:CSA(60.8) film: (A,C), 2D topographical and (B,D) and 3D topographical images of 20 μm and 6.8 μm , respectively, obtained in resonant mode. (E) Image acquired on the AFM support prior to performing the analysis.

3.3. Thermal stability

According to the TGA data (Figures 8 and S9 in Supplementary Material), thermal decomposition of all the CA:CSA(X) electrolytes with $X \leq 82.3$ invariably occurs in two steps: 1) loss of water below 120 °C (5-10% weight loss) and 2) major thermal degradation with onset at 120-140 °C.

As the pH decreases, the strength of the electrostatic interaction first increases, and then, at very low pH values, decreases due to the increment of the repulsion of the protonated groups. A decrease in the water content of the solids is an indication of a more compact CSA conformation [63,76,77,78], which is prone to increase any repulsion effect on the protonated groups. On the other hand, Volpi *et al.* pointed out that the presence of acidic compounds, such as the CA used in this work, leads to an acid-catalyzed hydrolysis of the glycosidic linkages at moderate temperatures [79]. Such a mechanism might help explaining what is happening here. Moreover, the comparison of the degradation onset values of the CA:CSA(X) compounds with those found for DESs obtained from combinations of simple sugars and organic acids [26,28], further suggests a thermal decomposition mechanism affecting primarily the CSA structure, as no gain in thermal stability was observed when a simple sugar is replaced by a polysaccharide, such as CSA.

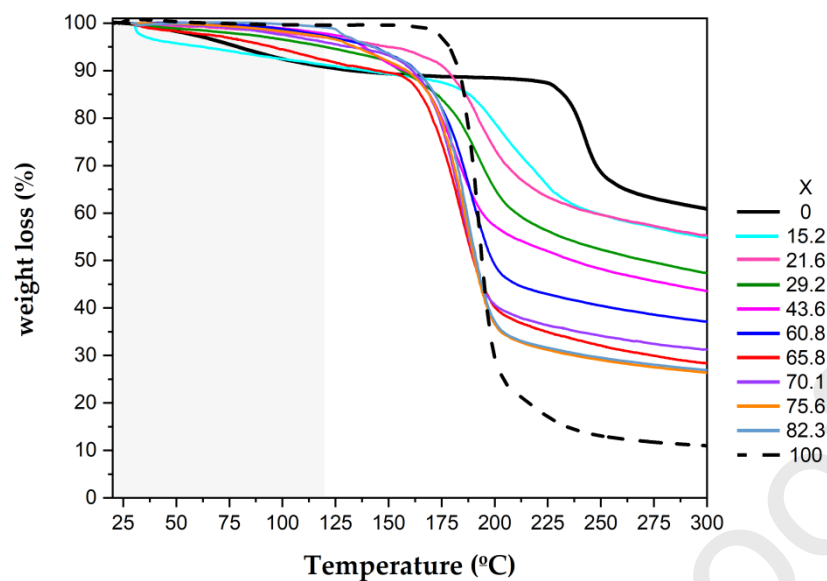


Figure 8. TGA curves for CA, CSA and CA:CSA(X) electrolytes with $X < 83.4$ in the 30-300 °C range

3.4. Ionic conductivity

The Arrhenius conductivity plot of CA:CSA(X) electrolytes with $X = 43.6, 60.8$ and 82.3 , shown in Figures 9A and S10 (in Supplementary Material), for data, demonstrates that at room temperature CA:CSA(43.6) has a lower ionic than the polysaccharide precursor, whereas the remaining two films tested ($X = 60.8$ and 82.3) feature a proton conductivity higher than CSA. These results, along with those observed for the powdered samples (Figure S14 in Supplementary Material), indicate that the proton conductivity enhancement effect due to the presence of CA is only observable in a limited range of X . Low and high X values give rise to electrolytes with poorer ionic conductivity.

The effect of composition can be rationalised admitting chemical interaction between the mixture components. Indeed, CA is expected to interact with the anionic groups present in CSA.

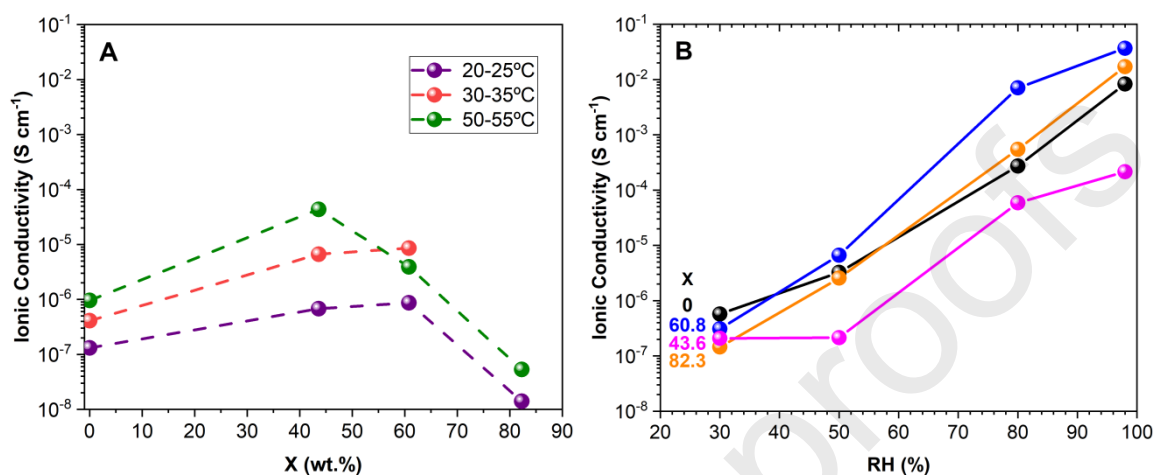


Figure 9. Ionic conductivity isotherms obtained (A) at a relative humidity lower than 30 % and (B) relative humidity dependence of the ionic conductivity under different RH at 25 °C for CSA and CA:CSA(X), with X = 0, 43.6, 60.8 and 82.3.

As the CA molecule possesses two terminal carboxylic groups, the interaction probably occurs through cross-linking between the carboxylic groups of CA and the anionic groups present in the polysaccharide (carboxylate and sulfate groups, for low and high CA content, respectively) (Figure S11, in Supplementary Material). Similar reaction schemes have been proposed for electrolyte systems formed between chitosan and organic acids [47–49,80]. The addition of CA to the CSA allows the formation of intermolecular interactions between CSA and CA at the expense of the existing intermolecular interactions between the amide and the carboxylic groups of the polysaccharide, resulting in the enlargement of the distance between the CSA chains

with the increase of CA content and in an increase of the tensile strength of the electrolyte [47].

The ionic conductivity data can be explained in terms of the content of CA present in the electrolytes.

As indicated in Section 3.1, a freshly prepared solution of CSA had a pH of 6.0. The addition of CA leads to a decrease of the pH, and thus should lead to an increase of ionic conductivity. However, with the CA acting as a cross-linker (Figure S11), the low content of CA might not be enough to improve on the mechanical properties of the CSA films. The lower ionic conductivity values observed for CA:CSA(43.6) can thus be attributed to a low content of CA, which leads to the formation of films with poor mechanical properties and low intermolecular interactions between CSA and CA [47,65,66]. In the same way, the enhancement in ionic conductivity observed for CA:CSA(X) electrolytes with $X = 60.8$ and 82.3 can be explained with the higher amount of CA which led to more compact and stronger films. CA:CSA(60.8), which yields the highest proton conductivity at room temperature, has been found to be one of the most homogenous films prepared out of the whole series here described, with the spectroscopic data indicating no clear excess of either CSA or CA. On the other hand, CA:CSA(82.3) has been shown to possess both an excess of CA, as indicated in Section 3.2., and a remarkably different morphology than that observed for the remaining electrolytes of this series. This particular sample, which seems to be at the transition between the formation of the film and the powders formed at higher CA content, still

possesses enough amorphous content, as observed by POM measurements, which is believed to be responsible for the proton conductivity.

The temperature dependence of the ionic conductivity is irregular (Figure S10 in Supplementary Material). The ionic conductivity increases for temperatures up to 50 °C, which coincides with the CSA gel-sol transition (Figure S8 in Supplementary Material). Above this transition temperature, the ionic conductivities decrease, probably due to the loss of mechanical properties. In addition, the CA:CSA(82.3) sample exhibits the highest proton conductivity at 50 °C.

The conductivity values measured at room temperature and under variable relative humidity (RH) are plotted in Figure 9B. The proton conductivity of the membranes is highly humidity-dependent, with values ranging from $1.4 \times 10^{-7} \text{ S cm}^{-1}$ for CA:CSA(82.3) at 30% RH to $3.7 \times 10^{-2} \text{ S cm}^{-1}$ for CA:CSA(60.8) at 98% RH, confirming that these membranes are highly hydrophilic. As expected, and in accordance with the results regarding the effect of temperature (Figure S10 in Supplementary Material), the electrolyte with the lowest CA content ($X = 43.6$) shows the lowest proton conductivity values for RH higher than 30%. At 98% RH the conductivity of CA:CSA(43.6) reaches $2.1 \times 10^{-4} \text{ S cm}^{-1}$, which is one order of magnitude lower than that measured for CSA. At RH higher than 50% the CA:CSA(60.8) film presents the highest proton conductivity. One would expect higher proton conductivities for CA:CSA(82.3), since according to EDS data all the sulfonic groups at the surface are protonated. However, both the spectroscopic and the morphologic data point to the presence of a secondary phase consisting of pure CA. The lower values here observed, which are also in accordance

with the ones seen in Figure 9A and S10, are consistent with the occurrence of secondary processes such as the CA dimerization observed in Section 3.2, and of a lower intermolecular interaction between the CA and CSA than the one observed for CA:CSA(60.8).

The higher conductivity of CA:CSA(60.8) may be probably related to the formation of a system with an amorphous structure and improved dimensional stability (crack-free), that contributes to the overall increase of proton mobility [47]. Such apparent inconsistency may also result from the viscous deformation of the membranes at high humidity, leading to uncontrolled changes of the geometric factor (e.g. the decrease of membrane thickness) used to estimate the conductivity. In fact, after the measurements at 98% RH the samples were found in a gel-like film, a fact that confirms the hydrophilic character of the materials and is a strong evidence that changes of the sample geometry may indeed occur during the measurements. These observations indicate that the CA:CSA(X) electrolytes may be not suitable for application in hydrogen/oxygen fuel cells, since they are not stable enough to withstand high humidity environments. The materials proposed here remain, however, suitable for other electroactive applications, where they can act as the ion-conducting layer in electrochromic materials or even batteries.

4. Concluding Remarks

While CSA is widely researched for biomedical applications, seldom work has been done in exploring its applicability as electroactive material. And yet, the presence of

sulfonic groups makes it an interesting option for these applications. This study aimed at understanding how CSA could function as a host polymer for PEs.

The combination of CSA with CA afforded materials shown to possess different properties, according to their specific mass ratio. The combination of CSA with CA led to the formation of whitish polycrystalline powders at high CA content, or transparent amorphous films at lower CA content. CA is shown to work as a cross-linker, interacting with the anionic groups present in CSA. The optimal CA mass ratio was observed for CA:CSA(60.8), with lower and higher CA mass ratios yielding PEs with worse mechanical properties and lower ionic conductivities.

For $X = 60.8$, SEM and AFM analysis indicated a practically homogenous film with some CA crystallites ranging from 0.88 to 2.6 μm . An ionic conductivity of about $10^{-7} \text{ S cm}^{-1}$ was measured near room temperature. At 50 $^{\circ}\text{C}$, CA:CSA(60.8) exhibited $10^{-5} \text{ S cm}^{-1}$, two orders of magnitude higher than the value observed for CSA. For $\text{RH} \geq 50\%$ CA:CSA(60.8) displayed higher ionic conductivities than the parent CSA (at 98% RH, 3.7×10^{-2} and $3.7 \times 10^{-3} \text{ S cm}^{-1}$, respectively).

The results reported here indicate that, although the present systems cannot be directly applied in a hydrogen/oxygen fuel cells, they can still be combined with an inorganic matrix in order to minimize their hydrophility. This study opens interesting prospects of research for CSA-based materials as electrolytes for solid state electrochemical devices, as long as their operation does not lead to the formation of water and does not require ionic conductivities as high as those needed in the case of batteries and fuel cells. Consequently, the present electrolyte system would be suitable,

for instance, for electrochemical devices. Moreover, although the materials here reported were obtained by combination of CSA with CA, this strategy could be virtually extended to any combination between an anionic polysaccharide (e.g., CS, hyaluronic acid or heparin) and any carboxylic acid, thereby offering new research possibilities. Indeed variables, such as the number of anionic groups and chemical composition of the monomeric unit, in the case of the polysaccharide, and the number of available protons and the geometry, in the case of the carboxylic acid molecule, can be explored in order to further customize new films.

Acknowledgments: Support by FCT in the framework of the Strategic Funding UID/FIS/04650/2013, UID/QUI/00686/2013 and UID/QUI/00686/2016 This work was funded by the R&D Project UniRCell-Unitised regenerative fuel cell for efficient renewable energy supply: from materials to device, with reference POCI-01-0145-FEDER-016422 and SAICTPAC/0032/2015, financed by the European Regional Development Fund (ERDF) through COMPETE 2020 – Operational Program for Competitiveness and Internationalization (POCI) and by the Foundation for Science and Technology (FCT) and CICECO-Aveiro Institute of Materials (UID/CTM/50011/2019), financed by national funds through the FCT/MEC. Is also acknowledged, as well as funding under projects UID/CTM/50025/2013, Pest-OE/QUI/UI0616/2014, and LUMECD (PTDC/CTM/NAN/0956/20149 and POCI-01-0145- FEDER-016884). F. M. Santos acknowledges a Post-PhD Fellow grant

supported by Project UniRcell. P. C. Barbosa employment contract is funded by national funds (OE), through FCT – Fundação para a Ciência e a Tecnologia, I.P., in the scope of the framework contract foreseen in the numbers 4, 5 and 6 of the article 23, of the Decree-Law 57/2016, of August 29, changed by Law 57/2017, of July 19. R. F. P. Pereira Post-PhD fellow was funded by FCT (SFRH/BPD/87759/2012). S. C. Nunes was funded by FCT projects (Post-PhD Fellowships of UniRCell and LUMECD projects).

Data availability

The raw/processed data required to reproduce these findings cannot be shared at this time as the data also forms part of an ongoing study.

References

- [1] United Nations World Commission on Environment and Development, Brundtland Report: Our Common Future, Oxford University Press, Oxford, 1987.
- [2] United Nations, The sustainable development goals report 2016, United Nations, New York, USA, 2016. doi:10.29171/azu_acku_pamphlet_k3240_s878_2016.
- [3] M. Irimia-Vladu, “Green” electronics: biodegradable and biocompatible materials and devices for sustainable future, *Chem. Soc. Rev.* 43 (2014) 588–610. doi:10.1039/c3cs60235d.
- [4] A. Kafy, H.-U. Ko, H.C. Kim, S. Mun, L. Zhai, J. Kim, Renewable smart materials, *Smart Mater. Struct.* 25 (2016) 073001 (14p). doi:10.1088/0964-1726/25/7/073001.
- [5] S. Admassie, F.N. Ajjan, A. Elfwing, O. Inganäs, Biopolymer hybrid electrodes for scalable electricity storage, *Mater. Horizons.* 3 (2016) 174–185. doi:10.1039/c5mh00261c.

- [6] F.M. Gray, *Solid Polymer Electrolytes: Fundamentals and Technological Applications*, VCH Publishers, Inc., New York, USA, 1991.
- [7] C.A.C. Sequeira, D.M.F. Santos, *Introduction to Polymer Electrolyte Materials*, in: C.A.C. Sequeira, D.M.F. Santos (Eds.), *Polym. Electrolytes Fundam. Appl.*, Woodhead Publishing, Oxford, UK, 2010: pp. 3–61. doi:10.1533/9781845699772.1.3.
- [8] P.K. Singh, R.K. Nagarale, S.P. Pandey, H.W. Rhee, B. Bhattacharya, *Present status of solid state photoelectrochemical solar cells and dye sensitized solar cells using PEO-based polymer electrolytes*, *Adv. Nat. Sci. Nanosci. Nanotechnol.* 2 (2011) 023002 (13p). doi:10.1088/2043-6262/2/2/023002.
- [9] A. Kavanagh, R. Byrne, D. Diamond, K.J. Fraser, *Stimuli responsive ionogels for sensing applications – an overview*, *Membranes (Basel)*. 2 (2012) 16–39. doi:10.3390/membranes2010016.
- [10] H. Gao, K. Lian, *Proton-conducting polymer electrolytes and their applications in solid supercapacitors: a review*, *RSC Adv.* 4 (2014) 33091–33113. doi:10.1039/C4RA05151C.
- [11] A. Manthiram, X. Yu, S. Wang, *Lithium battery chemistries enabled by solid-state electrolytes*, *Nat. Rev. Mater.* 2 (2017) Article nr. 16103 (16p). doi:10.1038/natrevmats.2016.103.
- [12] V.L. Finkenstadt, *Natural polysaccharides as electroactive polymers*, *Appl. Microbiol. Biotechnol.* 67 (2005) 735–745. doi:10.1007/s00253-005-1931-4.
- [13] M.J. Neto, F. Sentanin, J.M.S.S. Esperança, M.J. Medeiros, A. Pawlicka, V. de Z. Bermudez, et al., *Gellan gum - Ionic liquid membranes for electrochromic device application*, *Solid State Ionics*. 274 (2015) 64–70. doi:10.1016/j.ssi.2015.02.011.

- [14] S.C. Nunes, R.F.P. Pereira, N. Sousa, M.M. Silva, P. Almeida, F.M.L. Figueiredo, et al., Eco-friendly red seaweed-derived electrolytes for electrochemical devices, *Adv. Sustain. Syst.* 1 (2017) 1700070 (17 p.). doi:10.1002/adsu.201700070.
- [15] C. Zhong, Y. Deng, A.F. Roudsari, A. Kapetanovic, M.P. Anantram, M. Rolandi, A polysaccharide bioprotonic field-effect transistor, *Nat. Commun.* 2 (2011) Article Nr. 476 (5 pages). doi:10.1038/ncomms1489.
- [16] J. Ma, Y. Sahai, Chitosan biopolymer for fuel cell applications, *Carbohydr. Polym.* 92 (2013) 955–975. doi:10.1016/j.carbpol.2012.10.015.
- [17] M.F. Shukur, M.F.Z. Kadir, Electrical and transport properties of NH₄Br-doped cornstarch-based solid biopolymer electrolyte, *Ionics (Kiel)*. 21 (2014) 111–124. doi:10.1007/s11581-014-1157-5.
- [18] M.N. Chai, M.I.N. Isa, Novel proton conducting solid bio-polymer electrolytes based on carboxymethyl cellulose doped with oleic acid and plasticized with glycerol, *Sci. Rep.* 6 (2016) Article Nr. 27328 (7pages). doi:10.1038/srep27328.
- [19] F.F. Simas-Tosin, A. Grein-Iankovski, M. Vidotti, I.C. Riegel-Vidotti, Polysaccharides as green biodegradable platforms for building-up electroactive composite materials: an overview, in: V.K. Thakur, M.K. Thakur, M.R. Kessler (Eds.), *Handb. Compos. from Renew. Mater.*, John Wiley & Sons, Inc, Beverly, USA, 2017: pp. 377–417. doi: 10.1002/9781119441632.ch97.
- [20] A. Takada, J.I. Kadokawa, Fabrication and characterization of polysaccharide ion gels with ionic liquids and their further conversion into value-added sustainable materials, *Biomolecules*. 5 (2015) 244–262. doi:10.3390/biom5010244.

- [21] T.P. Thuy Pham, C.W. Cho, Y.S. Yun, Environmental fate and toxicity of ionic liquids: a review, *Water Res.* 44 (2010) 352–372. doi:10.1016/j.watres.2009.09.030.
- [22] M. Amde, J.F. Liu, L. Pang, Environmental application, fate, effects, and concerns of ionic liquids: a review, *Environ. Sci. Technol.* 49 (2015) 12611–12627. doi:10.1021/acs.est.5b03123.
- [23] M.E. Heckenbach, F.N. Romero, M.D. Green, R.U. Halden, Chemosphere meta-analysis of ionic liquid literature and toxicology, *Chemosphere.* 150 (2016) 266–274. doi:10.1016/j.chemosphere.2016.02.029.
- [24] M.A. Cardoso, R. Leones, L.C. Rodrigues, M. Fernandes, F.L. Figueiredo, S.C. Nunes, et al., Di-ureasil hybrid electrolytes incorporating a new proton ionic liquid, *ChemElectroChem.* 3 (2016) 783–789. doi:10.1002/celec.201500557.
- [25] Q. Zhang, K. De Oliveira Vigier, S. Royer, F. Jérôme, Deep eutectic solvents: syntheses, properties and applications., *Chem. Soc. Rev.* 41 (2012) 7108–7146. doi:10.1039/c2cs35178a.
- [26] Y. Dai, J. van Spronsen, G.J. Witkamp, R. Verpoorte, Y.H. Choi, Natural deep eutectic solvents as new potential media for green technology, *Anal. Chim. Acta.* 766 (2013) 61–68. doi:10.1016/j.aca.2012.12.019.
- [27] M. Francisco, A. Van Den Bruinhorst, M.C. Kroon, Low-transition-temperature mixtures (LTTMs): A new generation of designer solvents, *Angew. Chemie - Int. Ed.* 52 (2013) 3074–3085. doi:10.1002/anie.201207548.
- [28] R. Craveiro, I. Aroso, V. Flammia, T. Carvalho, M.T. Viciosa, M. Dionísio, et al., Properties and thermal behavior of natural deep eutectic solvents, *J. Mol. Liq.* 215 (2016) 534–540. doi:10.1016/j.molliq.2016.01.038.

- [29] Y. Liu, J.B. Friesen, J.B. McAlpine, D.C. Lankin, S.N. Chen, G.F. Pauli, Natural deep eutectic solvents: properties, applications, and perspectives, *J. Nat. Prod.* 81 (2018) 679–690. doi:10.1021/acs.jnatprod.7b00945.
- [30] W.T. Winter, S. Arnott, D.H. Isaac, E.D.T. Atkins, Chondroitin 4-sulfate: the structure of a sulfated glycosaminoglycan, *J. Mol. Biol.* 125 (1978) 1–19. doi:10.1016/0022-2836(78)90251-6.
- [31] R. Leones, F. Sentanin, S.C. Nunes, J.M.S.S. Esperança, M.C. Gonçalves, A. Pawlicka, et al., Effect of the alkyl chain length of the ionic liquid anion on polymer electrolytes properties, *Electrochim. Acta.* 184 (2015) 171–178. doi:10.1016/j.electacta.2015.09.163.
- [32] B. Chakrabarti, J.W. Park, E.S. Stevens, Glycosaminoglycans: structure and interaction, *CRC Crit. Rev. Biochem.* 8 (1980) 225–313. doi:10.3109/10409238009102572.
- [33] R.M. Lauder, Chondroitin sulphate: a complex molecule with potential impacts on a wide range of biological systems, *Complement. Ther. Med.* 17 (2009) 56–62. doi:10.1016/j.ctim.2008.08.004.
- [34] D.A. Wang, S. Varghese, B. Sharma, I. Strehin, S. Fermanian, J. Gorham, et al., Multifunctional chondroitin sulphate for cartilage tissue-biomaterial integration, *Nat. Mater.* 6 (2007) 385–392. doi:10.1038/nmat1890.
- [35] I.G.F. Gilbert, N.A. Myers, Metal binding properties of chondroitin sulphate, *Biochim. Biophys. Acta.* 42 (1960) 469–475. doi:10.1016/0006-3002(60)90825-8.
- [36] S. Hirano, C. Mizutani, R. Yamaguchi, O. Miura, Formation of the polyelectrolyte complexes of some acidic glycosaminoglycans with partially N-acylated chitosans, *Biopolymers.* 17 (1978) 805–810. doi:10.1002/bip.1978.360170320.

- [37] A. Denuzière, D. Ferrier, A. Domard, D. Ferrief, A. Domard, Chitosan-chondroitin sulfate and chitosan-hyaluronate polyelectrolyte complexes. Physico-chemical aspects, *Carbohydr. Polym.* 29 (1996) 317–323. doi:10.1016/S0144-8617(96)00035-5.
- [38] W. Bin Chen, L.F. Wang, J.S. Chen, S.Y. Fan, Characterization of polyelectrolyte complexes between chondroitin sulfate and chitosan in the solid state, *J. Biomed. Mater. Res. - Part A.* 75 (2005) 128–137. doi:10.1002/jbm.a.30393.
- [39] C. Alvarez-Lorenzo, B. Blanco-Fernandez, A.M. Puga, A. Concheiro, Crosslinked ionic polysaccharides for stimuli-sensitive drug delivery, *Adv. Drug Deliv. Rev.* 65 (2013) 1148–1171. doi:10.1016/j.addr.2013.04.016.
- [40] C.S. Nunes, K.B. Rufato, P.R. Souza, E.A.M.S. de Almeida, M.J.V. da Silva, D.B. Scariot, et al., Chitosan/chondroitin sulfate hydrogels prepared in [Hmim][HSO₄] ionic liquid, *Carbohydr. Polym.* 170 (2017) 99–106. doi:10.1016/j.carbpol.2017.04.073.
- [41] S. Yamada, K. Sugahara, Potential therapeutic application of chondroitin sulfate/dermatan sulfate., *Curr. Drug Discov. Technol.* 5 (2008) 289–301. doi:10.2174/157016308786733564.
- [42] A. Köwitsch, G. Zhou, T. Groth, Medical application of glycosaminoglycans: a review, *J. Tissue Eng. Regen. Med.* 12 (2018) e23–e41. doi:10.1002/term.2398.
- [43] Y. Li, J. Rodrigues, H. Tomás, Injectable and biodegradable hydrogels: gelation, biodegradation and biomedical applications, *Chem. Soc. Rev.* 41 (2012) 2193–2221. doi:10.1039/c1cs15203c.
- [44] R. Ciriminna, F. Meneguzzo, R. Delisi, M. Pagliaro, Citric acid: emerging applications of key biotechnology industrial product, *Chem. Cent. J.* 11 (2017) 22 (9 p.). doi:

10.1186/s13065-017-0251-y.

- [45] M. Espino, M. de los Ángeles Fernández, F.J.V. Gomez, M.F. Silva, Natural designer solvents for greening analytical chemistry, *TrAC - Trends Anal. Chem.* 76 (2016) 126–136. doi:10.1016/j.trac.2015.11.006.
- [46] P. Jia, H. Xia, K. Tang, Y. Zhou, Plasticizers derived from biomass resources: a short review, *Polymers (Basel)*. 10 (2018) 1303 (27 pp). doi:10.3390/polym10121303.
- [47] Y. Yang, H. Gao, L. Zheng, Anhydrous proton exchange membranes at elevated temperatures: Effect of protic ionic liquids and crosslinker on proton conductivity, *RSC Adv.* 5 (2015) 17683–17689. doi:10.1039/c4ra16106h.
- [48] I.A. Fadzallah, S.R. Majid, M.A. Careem, A.K. Arof, A study on ionic interactions in chitosan–oxalic acid polymer electrolyte membranes, *J. Memb. Sci.* 463 (2014) 65–72. doi:10.1016/j.memsci.2014.03.044.
- [49] I.A. Fadzallah, I.M. Noor, M.A. Careem, A.K. Arof, Investigation of transport properties of chitosan-based electrolytes utilizing impedance spectroscopy, *Ionics (Kiel)*. 22 (2016) 1635–1645. doi:10.1007/s11581-016-1687-0.
- [50] E. Prokhorov, G. Luna-Bárceñas, J.B. González-Campos, Y. Kovalenko, Z.Y. García-Carvajal, J. Mota-Morales, Proton conductivity and relaxation properties of chitosan-acetate films, *Electrochim. Acta.* 215 (2016) 600–608. doi:10.1016/j.electacta.2016.08.148.
- [51] Y. Zhao, Z. Jiang, L. Xiao, T. Xu, S. Qiao, H. Wu, Chitosan membranes filled with biomimetic mineralized hydroxyapatite for enhanced proton conductivity, *Solid State Ionics*. 187 (2011) 33–38. doi:10.1016/j.ssi.2011.01.019.

- [52] B. Larsson, M. Nilsson, H. Tjälve, The binding of inorganic and organic cations and H⁺ to cartilage in vitro, *Biochem. Pharmacol.* 30 (1981) 2963–2970. doi:10.1016/0006-2952(81)90260-4.
- [53] A.M.N. Silva, X. Kong, R.C. Hider, Determination of the pK_a value of the hydroxyl group in the α -hydroxycarboxylates citrate, malate and lactate by ¹³C NMR: Implications for metal coordination in biological systems, *BioMetals.* 22 (2009) 771–778. doi:10.1007/s10534-009-9224-5.
- [54] C.Y. Wong, W.Y. Wong, R.G. Walvekar, K.S. Loh, M. Khalid, K.L. Lim, Effect of deep eutectic solvent in proton conduction and thermal behaviour of chitosan-based membrane, *J. Mol. Liq.* 269 (2018) 675–683. doi:10.1016/j.molliq.2018.08.102.
- [55] J.F. Piai, L.C. Lopes, A.R. Fajardo, A.F. Rubira, E.C. Muniz, Kinetic study of chondroitin sulphate release from Chondroitin sulphate/chitosan complex hydrogel, *J. Mol. Liq.* 156 (2010) 28–32. doi:10.1016/j.molliq.2010.05.017.
- [56] S.M. Best, M.J. Duer, D.G. Reid, E.R. Wise, S. Zou, Towards a model of the mineral-organic interface in bone: NMR of the structure of synthetic glycosaminoglycan- and polyaspartate-calcium phosphate composites, *Magn. Reson. Chem.* 46 (2008) 323–329. doi:10.1002/mrc.2168.
- [57] V.H. Pomin, NMR chemical shifts in structural biology of glycosaminoglycans, *Anal. Chem.* 86 (2014) 65–94. doi:10.1021/ac401791h.
- [58] J.W. Fischer, L.H. Merwin, R.A. Nissan, NMR investigation of the thermolysis of citric acid, *Appl. Spectrosc.* 49 (1995) 120–126. doi:10.1366/0003702953963229.
- [59] J.W. Mullin, C.L. Leci, Evidence of molecular cluster formation in supersaturated

solutions of citric acid, *Philos. Mag.* 19 (1969) 1075–1077. doi:10.1080/14786436908225872.

- [60] G.K. Hamer, A.S. Perlin, A ^{13}C -N.M.R. spectral study of chondroitin sulfates A, B, and C: evidence of heterogeneity., *Carbohydr. Res.* 49 (1976) 37–48. doi: 10.1016/S0008-6215(00)83123-7.
- [61] S.M. Bociek, A.H. Darke, D. Welti, D.A. Rees, The ^{13}C -NMR spectra of hyaluronate and chondroitin sulphates: further evidence on an alkali-induced conformation change, *Eur. J. Biochem.* 109 (1980) 447–456. doi:10.1111/j.1432-1033.1980.tb04814.x.
- [62] J. Schiller, L. Naji, D. Huster, J. Kaufmann, K.A. Arnold, ^1H and ^{13}C HR-MAS NMR investigations on native and enzymatically digested bovine nasal cartilage, *MAGMA*. 13 (2001) 19–27. doi:10.1007/BF02668647.
- [63] A.R. Fajardo, J.F. Piai, A.F. Rubira, E.C. Muniz, Time- and pH-dependent self-rearrangement of a swollen polymer network based on polyelectrolytes complexes of chitosan/chondroitin sulfate, *Carbohydr. Polym.* 80 (2010) 934–943. doi:10.1016/j.carbpol.2010.01.009.
- [64] M. Criado, J.M. Rey, C. Mijangos, R. Hernández, Double-membrane thermoresponsive hydrogels from gelatin and chondroitin sulphate with enhanced mechanical properties, *RSC Adv.* 6 (2016) 105821–105826. doi:10.1039/c6ra25053j.
- [65] A.L. Kolesnikov, Y.A. Budkov, E.A. Nogovitsyn Coarse-grained model of glycosaminoglycans in aqueous salt solutions. A field-theoretical approach, *J. Phys. Chem. B* 118 (2014) 13037-13049. doi: 10.1021/jp503749a
- [66] E. A. Nogovitsin, Yu. A. Budkov, Self-consistent field theory investigation of the behavior of hyaluronic acid chains in aqueous salt solutions, *Physica A* 391 (2012) 2507-2517. doi:

10.1016/j.physa.2011.12.040.

- [67] R. Anedda, C. Cannas, A. Musinu, G. Pinna, G. Piccaluga, M. Casu, A two-stage citric acid-sol/gel synthesis of ZnO/SiO₂ nanocomposites: study of precursors and final products, *J. Nanoparticles Res.* 10 (2008) 107–120. doi:10.1007/s11051-007-9235-5.
- [68] S. Brézillon, V. Untereiner, L. Lovergne, I. Tadeo, R. Noguera, F.X. Maquart, et al., Glycosaminoglycan profiling in different cell types using infrared spectroscopy and imaging, *Anal. Bioanal. Chem.* 406 (2014) 5795–5803. doi:10.1007/s00216-014-7994-2.
- [69] S.F.D. Orr, Infra-red spectroscopic studies of some polysaccharides, *Spectroscopy.* 14 (1954) 173–181. doi:10.1016/0006-3002(54)90156-0.
- [70] J.J. Cael, D.H. Isaac, J. Blackwell, J.L. Koenig, E.D.T. Atkins, J.K. Sheehan, Polarized infrared spectra of crystalline glycosaminoglycans, *Carbohydr. Res.* 50 (1976) 169–179. doi:10.1016/S0008-6215(00)83848-3.
- [71] B. Casu, A.J. Cifonelli, A.S. Perlin, Infrared spectra of glycosaminoglycans in deuterium oxide and deuterium chloride solution: quantitative evaluation of uronic acid and acetamidodeoxyhexose moieties, *Carbohydr. Res.* 63 (1978) 13–27. doi:10.1016/S0008-6215(00)80925-8.
- [72] R. Servaty, J. Schiller, H. Binder, K.A. Arnold, Hydration of polymeric components of cartilage - An infrared spectroscopic study on hyaluronic acid and chondroitin sulfate, *Int. J. Biol. Macromol.* 28 (2001) 121–127. doi:10.1016/S0141-8130(00)00161-6.
- [73] C. Djordjevic, M. Lee, E. Sinn, Oxoperoxo(citrato)- and dioxo(citrato)vanadates(V): synthesis, spectra, and structure of a hydroxyl oxygen bridged dimer K₂[VO(O₂)(C₆H₆O₇)]₂·2H₂O, *Inorg. Chem.* 380 (1989) 719–723. doi:10.1021/ic00303a022.

- [74] P. Tarakeshwar, S. Manogaran, Ground state vibrations of citric acid and the citrate trianion – an ab initio study, *Spectrochim. Acta Part A Mol. Spectrosc.* 50 (1994) 2327–2343. doi:10.1016/0584-8539(94)E0017-5.
- [75] S.A. Brandán, L.C. Bichara, H.E. Lans, E.G. Ferrer, M.B. Gramajo, Vibrational study and force field of the citric acid dimer based on the SQM methodology, *Adv. Phys. Chem.* 2011 (2011). doi:10.1155/2011/347072.
- [76] J.F. Piai, A.F. Rubira, E.C. Muniz, Self-assembly of a swollen chitosan/chondroitin sulfate hydrogel by outward diffusion of the chondroitin sulfate chains, *Acta Biomater.* 5 (2009) 2601–2609. doi:10.1016/j.actbio.2009.03.035.
- [77] A.R. Fajardo, L.C. Lopes, A.J.M. Valente, A.F. Rubira, E.C. Muniz, Effect of stoichiometry and pH on the structure and properties of chitosan/chondroitin sulfate complexes, *Colloid Polym. Sci.* 289 (2011) 1739–1748. doi:10.1007/s00396-011-2497-6.
- [78] M. Bathe, G.C. Rutledge, A.J. Grodzinsky, B. Tidor, A coarse-grained molecular model for glycosaminoglycans: application to chondroitin, chondroitin sulfate, and hyaluronic acid, *Biophys. J.* 88 (2005) 3870–3887. doi:10.1529/biophysj.104.058800.
- [79] N. Volpi, A. Mucci, L. Schenetti, Stability studies of chondroitin sulfate, *Carbohydr. Res.* 315 (1999) 345–349. doi:10.1016/S0008-6215(99)00034-8.
- [80] T. Gümüsoğlu, G.A. Ari, H. Deligöz, Investigation of salt addition and acid treatment effects on the transport properties of ionically cross-linked polyelectrolyte complex membranes based on chitosan and polyacrylic acid, *J. Memb. Sci.* 376 (2011) 25–34. doi:10.1016/j.memsci.2011.03.040.

Supplementary Material

Proton Conducting Electrolytes Composed of Chondroitin Sulfate Polysaccharide and Citric Acid

Filipe M. Santos^{a,*}, Paula C. Barbosa^b, Rui F. P. Pereira^c, M. M. Silva^c, Helena M.R. Gonçalves^{a,d}, Sílvia C. Nunes^{e, f}, Filipe Figueiredo^b, Artur J. M. Valente^g, Verónica de Zea Bermudez^{a*}

^a Department of Chemistry/CQ-VR, University of Trás-os-Montes e Alto Douro, 5001-801 Vila Real, Portugal;

^b Department of Materials and Ceramic Engineering/ CICECO – Aveiro Institute of Materials, University of Aveiro, 3810-193 Aveiro, Portugal;

^c Chemistry Center and Chemistry Department, University of Minho, 4710-057 Braga, Portugal;

^d REQUIMTE, Instituto Superior de Engenharia do Porto, 4200-072 Porto, Portugal;

^e Chemistry Department, University of Beira Interior, 6201-001 Covilhã, Portugal;

^f Department of Chemistry, University of Trás-os-Montes e Alto Douro, 5001-801 Vila Real,

^g Chemistry Department, University of Coimbra, Coimbra, Portugal;

* Correspondence: filipems@utad.pt (F.M.S); vbermude@utad.pt (V.d.Z.B.); Tel.: +351-259-350000 (V.d.Z.B.)

Experimental Data

Table S1. Experimental data on the synthesis of the CA:CSA(X) polyelectrolytes.

Sample (X)	v(CSA) (mL)	v(CA) (mL)
0 (CSA)	11.00	
15.2	9.00	0.14
21.6	9.00	0.27
29.2	9.00	0.30
43.6	10.00	0.63
60.8	8.00	1.00
70.1	9.00	1.70
75.6	8.00	2.00
82.3	8.00	3.00
83.4	8.00	3.25
84.4	8.00	3.50
86.1	6.00	3.00
90.3	6.00	4.50
92.5	5.00	5.00
93.7	5.00	6.00
100 (CA)		11.00

To prove that the CA:CSA(60.8) film mimicked the mold indentations, a replica was prepared and dried using a Teflon mold and a Falcon stopper as surfaces for the drying process. Despite the macroscopic visualization of the pattern on the Falcon stopper (number 1, Figure S1a), it was also possible to detect micrometer (Figure S1b) and sub-micrometer (Figure S1c) changes.

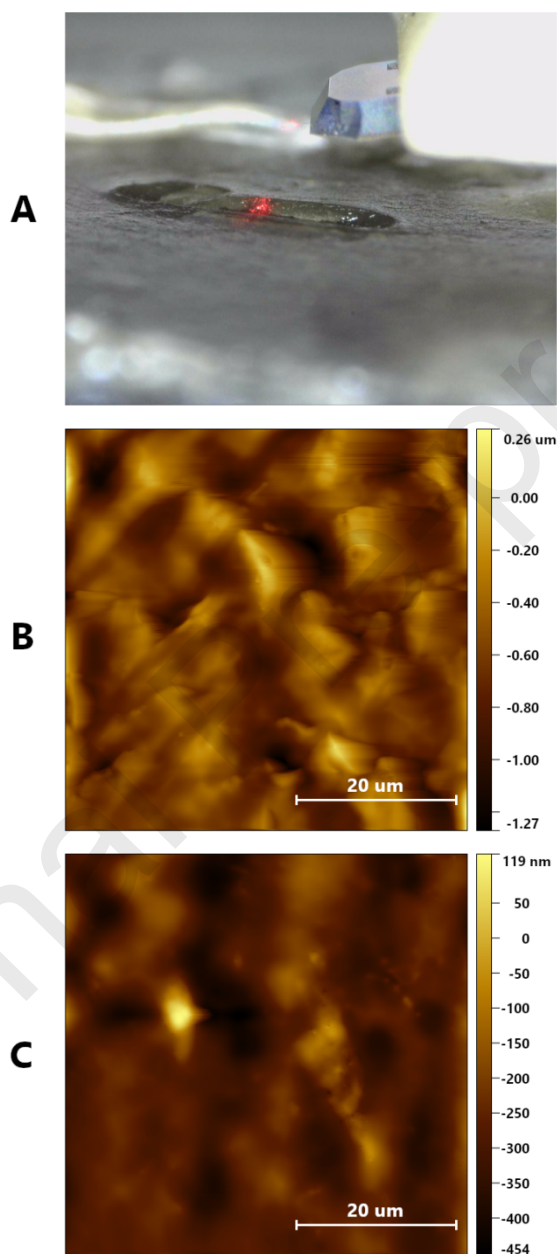


Figure S1: CA:CSA(60.8) film: a) Macroscopic image on the AFM support, and b) Micrometric topographical image of the film surface left to dry in contact with a Falcon stopper. c) Sub-micrometric topographical image of the film surface left to dry in contact with the Teflon mold.

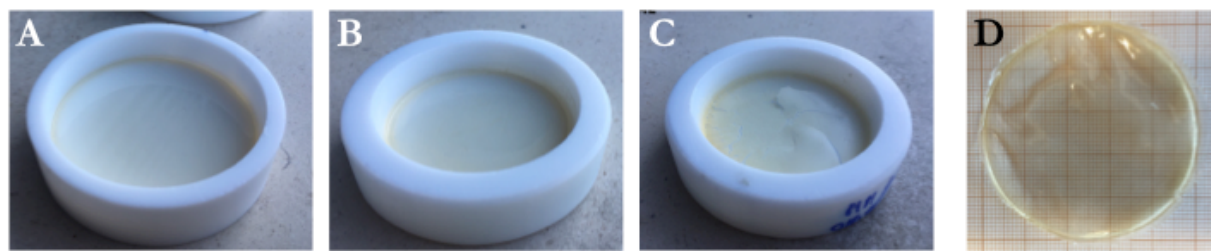


Figure S2. Selected CA:CSA(X) electrolyte films: (A) X = 60.8; (B) X = 29.2; (C) X = 15.2; (D) X = 60.8

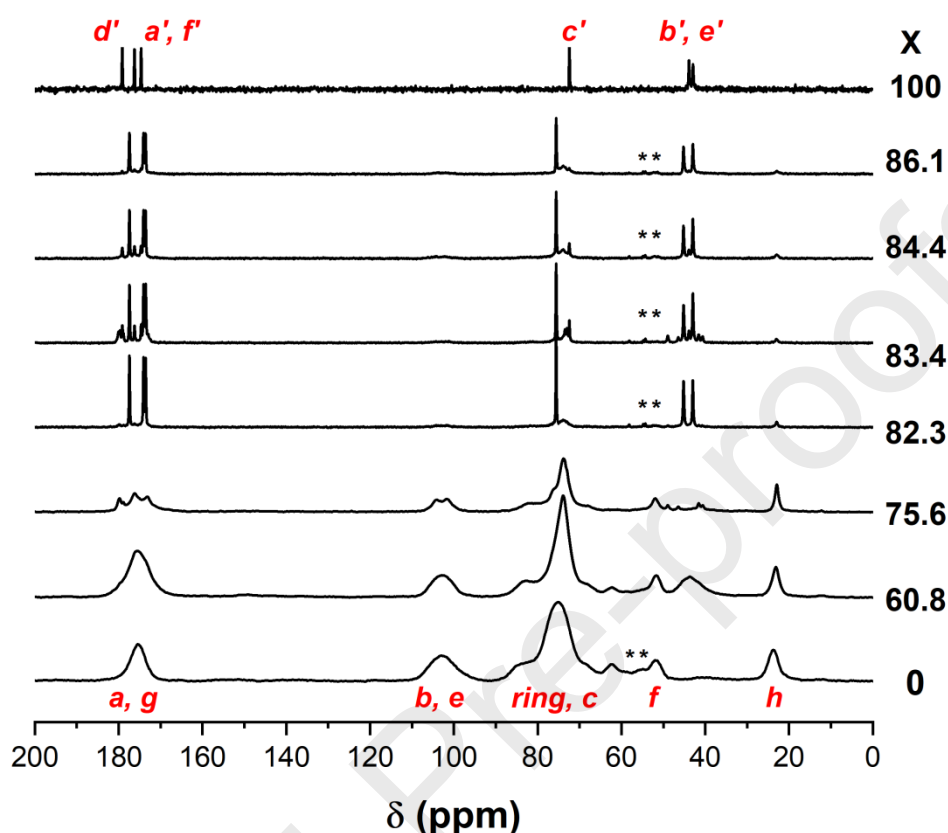
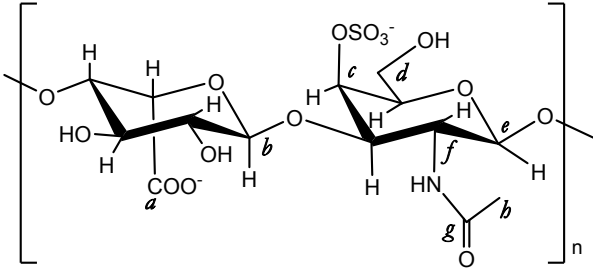
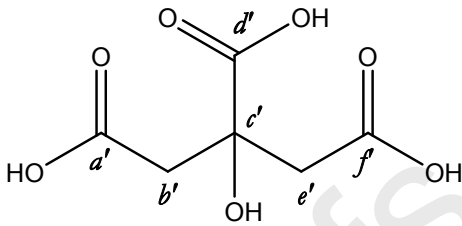
¹³C CP/MAS Spectroscopy

Figure S3. ¹³C CP/MAS NMR spectra of CSA, CA and selected spectra from CA:CSA electrolytes. (*) indicates a sideband.

The spectrum of CSA (Figure S2 and Table S2) presents a broad unresolved resonance at 175.4 ppm due to the carbonyl groups of the carboxylic (signal *a*, Table S2) and the amide (signal *g*) groups. The resonance at 102.8 ppm is due to the anomeric carbon (signals *b* and *e*), and that at 23.8 ppm is associated with the methyl group of the *N*-acetyl amide carbon (signal *h*). The broad resonance located at 75.0 ppm (as well as the shoulder at 83.9 ppm) is due to the various carbon atoms of the glycosidic ring and to the methylene carbon linked to the sulfonic group. The signals located at 51.6 and 62.3 ppm are attributed to the $-\text{CHNHCOCH}_3$ (signal *f*) and $-\text{CH}_2\text{OH}$ (signal *d*) present on the *N*-acetylgalactosamide monomer, respectively [1–4].

The ¹³C CP/MAS NMR spectrum of the anhydrous CA exhibits three resonances due to the carboxyl group at 179.2 (signal *d'*, corresponding to the central carboxylic group), 176.2 (signal *a'*) and 174.6 ppm (signal *f'*) (Figure S2 and Table S2), one resonance at 72.43 ppm corresponding to the central carbon atom in the molecule, and two resonances located at 43.9 and 42.9 ppm, assigned to the two methylene carbons (Figure S2 and Table S2). The splitting of the signals corresponding to the terminal carboxylic groups (signals *a'* and *f'*) and the methylene groups (signals *b'* and *e'*) observed, reflects a slightly different chemical environment [5,6]. Globally, the chemical shifts here observed correlate well with the literature [5,6].

Table S2. ^{13}C CP/MAS NMR Peak assignments for CSA and CA.

CHONDROITIN SULFATE		CITRIC ACID	
			
Chemical shift (ppm)	Signal assignment	Chemical shift (ppm)	Signal assignment
175.4	<i>a, g</i>	179.2	<i>d'</i>
102.8	<i>b, e</i>	176.2	<i>a'</i>
83.9 (sh)	Glycosidic ring, including <i>c</i>	174.6	<i>f'</i>
75.0		72.43	<i>c'</i>
62.3	<i>d</i>	43.9	<i>b'</i>
51.6	<i>f</i>	42.9	<i>e'</i>
23.8	<i>h</i>		

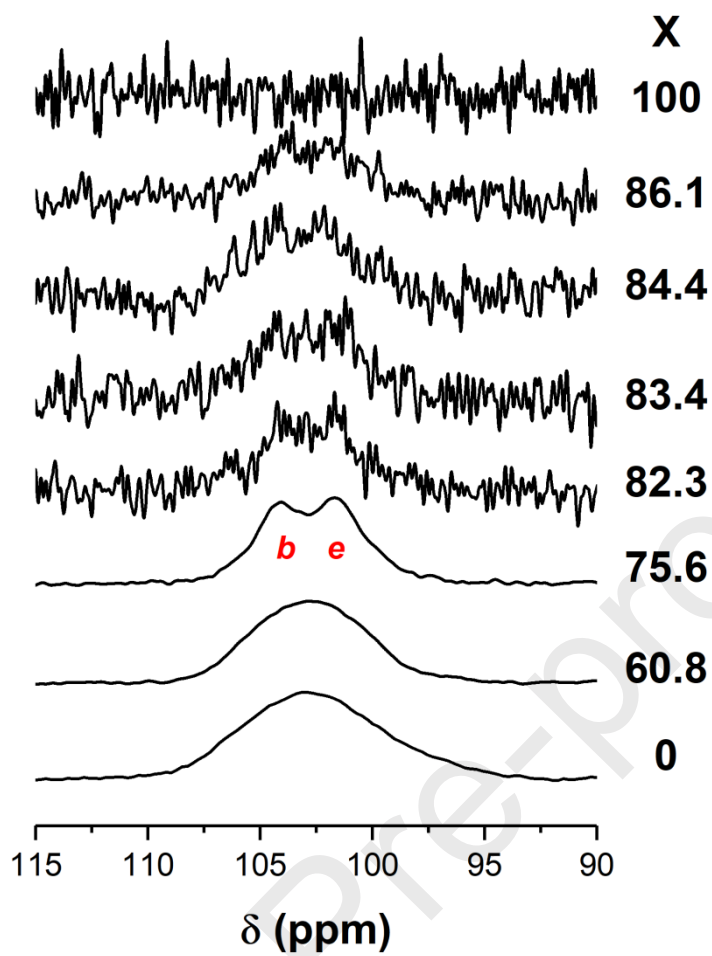


Figure S4. ^{13}C CP/MAS NMR spectra of CSA, CA and selected CA:CSA(X) electrolytes

ATR-FTIR Spectroscopy

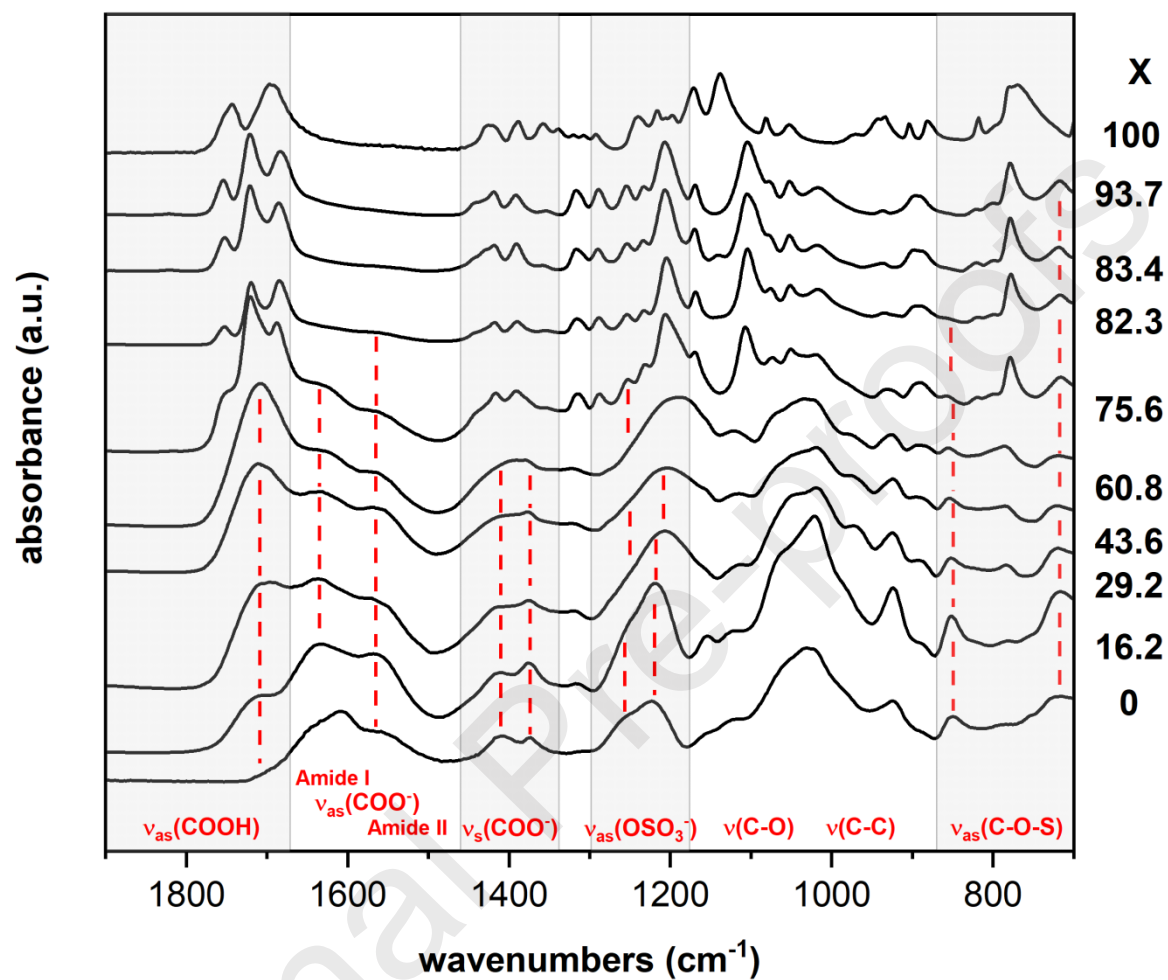


Figure S5. ATR-FTIR spectra of CSA, CA and selected CA:CSA(X) electrolytes.

Table S3. Relevant Infrared Data (in cm^{-1}) for CSA, CA and selected CA:CSA(X) electrolytes. **vs:** very strong; **v:** strong; **m:** medium; **sh:** shoulder

Band assignment	Polyelectrolytes									
	CSA	15.2	29.2	43.6	60.8	75.6	82.3	83.4	93.7	CA
$\nu_{\text{as}}(\text{COOH})$		1707 (sh)	1727 (sh)	1709 (m)	1727 (vs)	1729 (vs)	1720 (vs)	1722 (vs)	1722 (vs)	1743 (s)
					1686 (sh)	1687 (m)	1685 (s)	1685 (s)	1685 (s)	1693 (vs)
Amide I	1641 (sh)									
$\nu_{\text{as}}(\text{COO}^-)$	1607 (s)	1633 (vs)	1634 (vs)	1637 (m)	1633 (m)					
Amide II	1551 (sh)									
$\nu_{\text{s}}(\text{COO}^-)$	1408 (s)	1410 (s)	1418 (m)	1418 (m)	1416	1416 (m)	1419 (s)	1417 (s)	1418 (s)	1416 (s)
$\nu_{\text{as}}(\text{O-SO}_3^-)$	1224 (s)	1219 (s)	1206 (vs)	1207 (vs)	1206 (s)	1206 (s)	1206 (s)	1207 (s)	1206 (s)	
$\nu_{\text{as}}(\text{C-S-O})$	851 (s)	851 (s)	853 (m)	853 (m)	853 (m)	851 (sh)	852 (sh)	852 (sh)	852 (sh)	
	720 (m)	720 (m)	720 (m)	719 (m)	718 (m)	718 (m)	717 (m)	717 (sh)	717 (sh)	

Scanning Electron Microscopy and Electron Diffraction Scattering

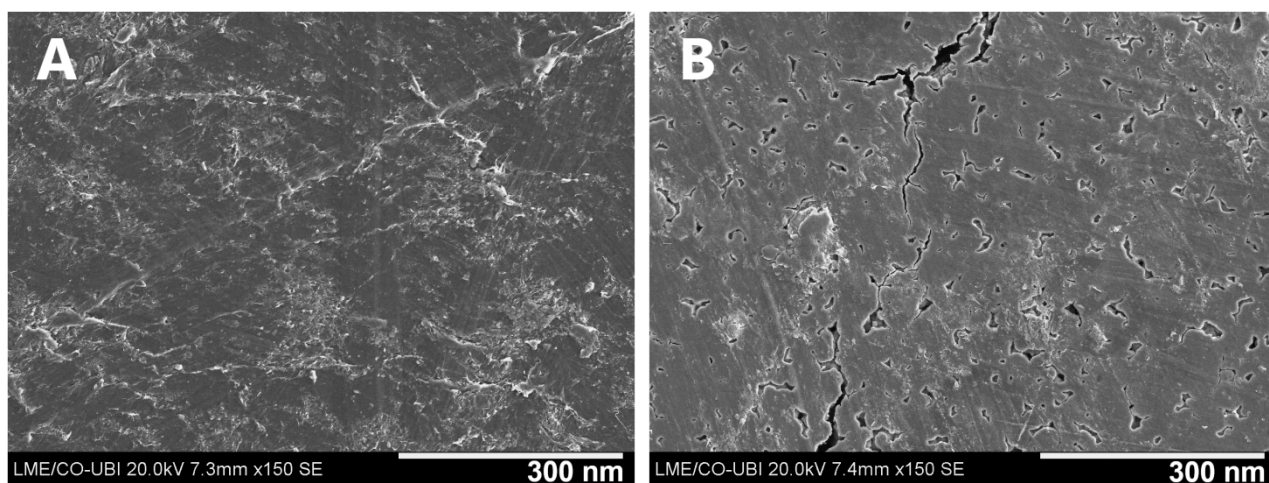


Figure S6. SEM images of the CA:CSA(X) films (bottom surface) with X = 75.6 and 82.3.

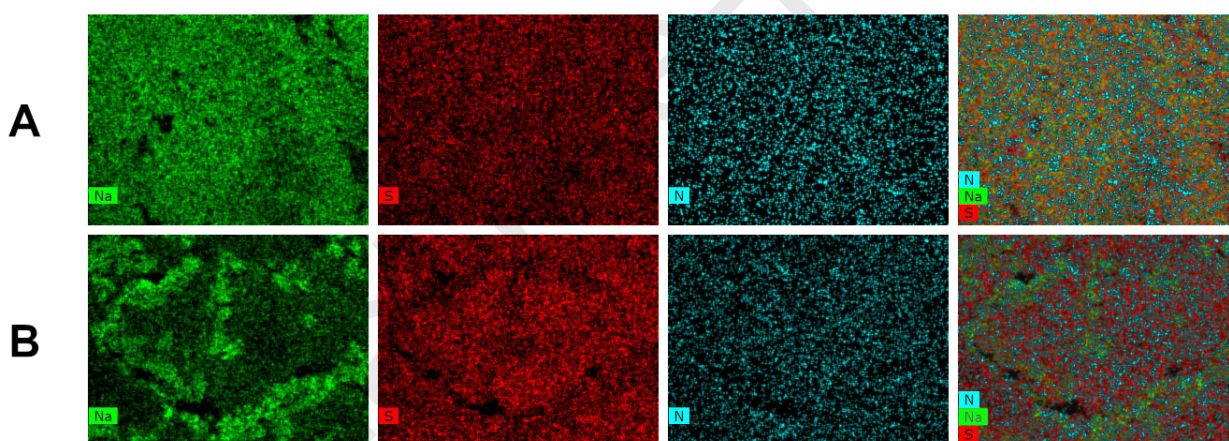


Figure S7. EDS distribution maps for CA:CSA(X) films (bottom surface) with X = 75.6 and 82.3.

At $X \geq 60.8$, variations first in the distribution of the Na^+ cations, and in the N element, associated with the amide group present in CSA, become apparent (Figure S7A). At $X = 75.6$ (Figure S7A), the distribution of Na^+ cations becomes increasingly heterogeneous, while the S mapping shows little to no difference. The absence of Na^+ cations in areas which contain sulfonic groups is due to the increase of the concentration of protons, setting a new equilibrium of charges, and further corroborating the ATR-FTIR findings regarding the chemical environment of the same sulfonic groups [7–10]. This shift in equilibrium becomes even more noticeable in Figure S7B, which shows the distribution of Na, N, and S atoms in an irregular film, revealing that most of the Na^+ cations are located mainly in areas where S appears to be more depleted, thus implying that all the sulfonic groups seen at the surface are protonated. The variation observed in the distribution of N can also be explained by the variation of the pH on the medium. As the pH progressively decreased, a

shift towards the protonated state of both the cationic and anionic groups of the CSA resulted. While the cationic $-\text{NH}_3^+$ groups are expected to repel each other, the anionic carboxylic and sulfonic groups will grow increasingly neutral, thus minimizing any electrostatic repulsion. Globally, the various changes undergone by the CSA structure induced changes in its conformation, due to the overall decrease of both inter- and intramolecular interactions, resulting in more compact conformations [9,11–13].

Journal Pre-proofs

Differential Scanning Calorimetry

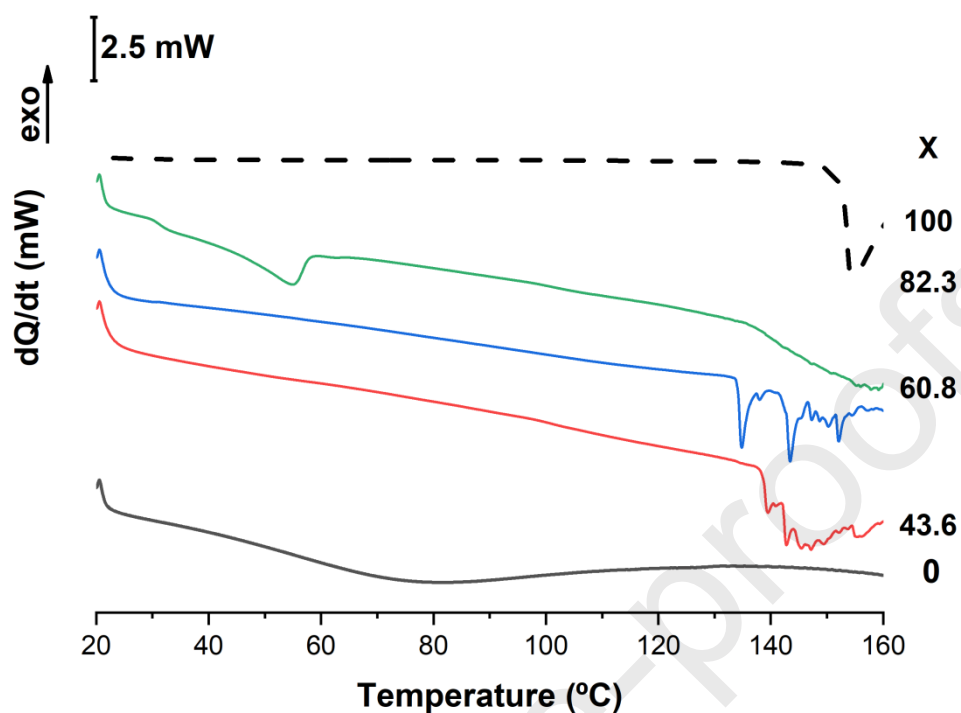


Figure S8. DSC curves of CSA, CA and selected CA:CSA(X) electrolytes.

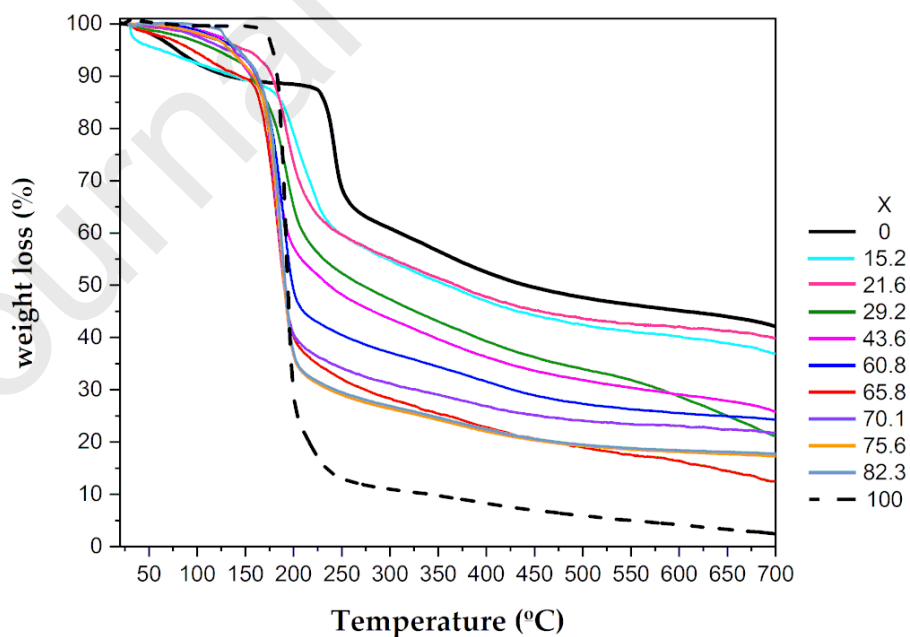
Thermogravimetric Data for Electrolytes with $X < 82.3\%$ 

Figure S9. TGA curves for CA, CSA and CA:CSA(X) electrolytes with $X < 83.4$ in the 30-700 °C range.

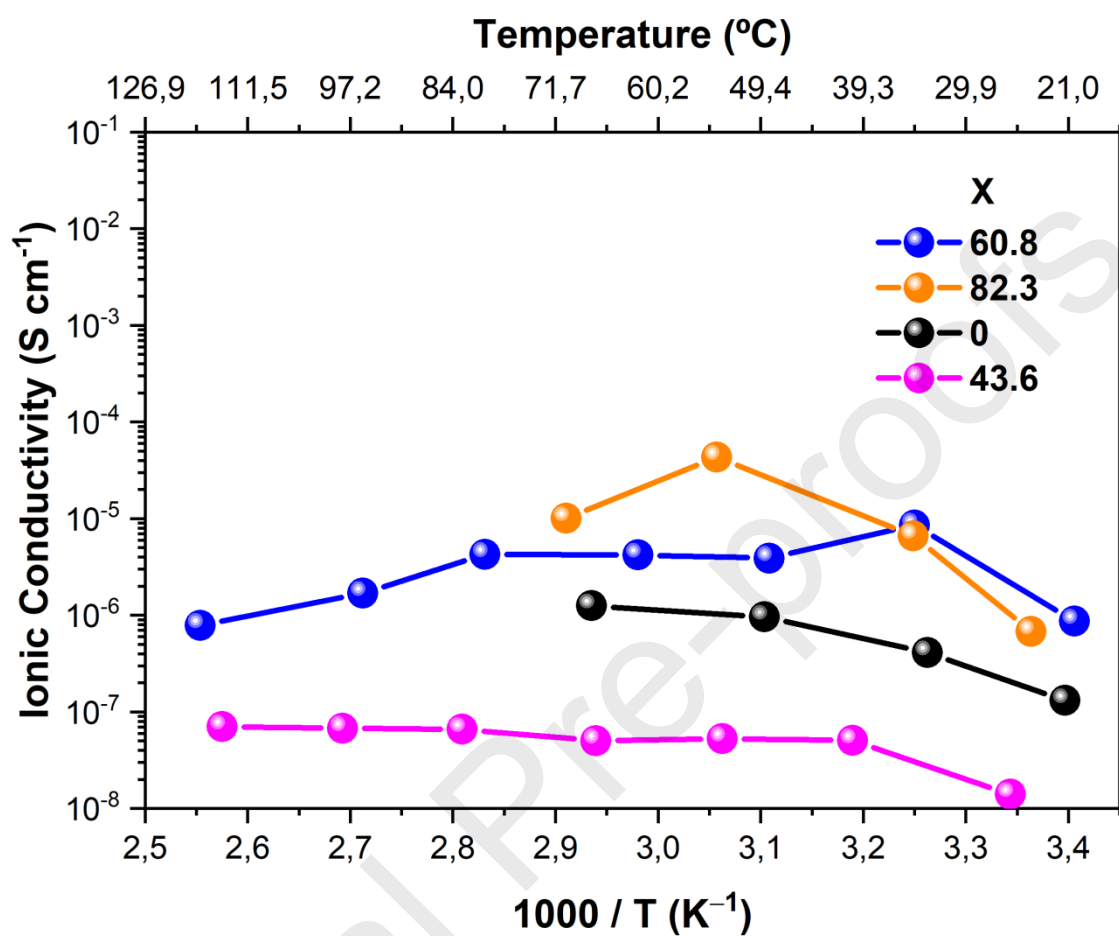
Ionic Conductivity for Electrolytes with $X < 82.3\%$ 

Figure S10. Arrhenius plots of the ionic conductivity at different temperatures for CSA and CA:CSA(X), with $X = 0, 43.6, 60.8$ and 82.3 .

Reaction Scheme

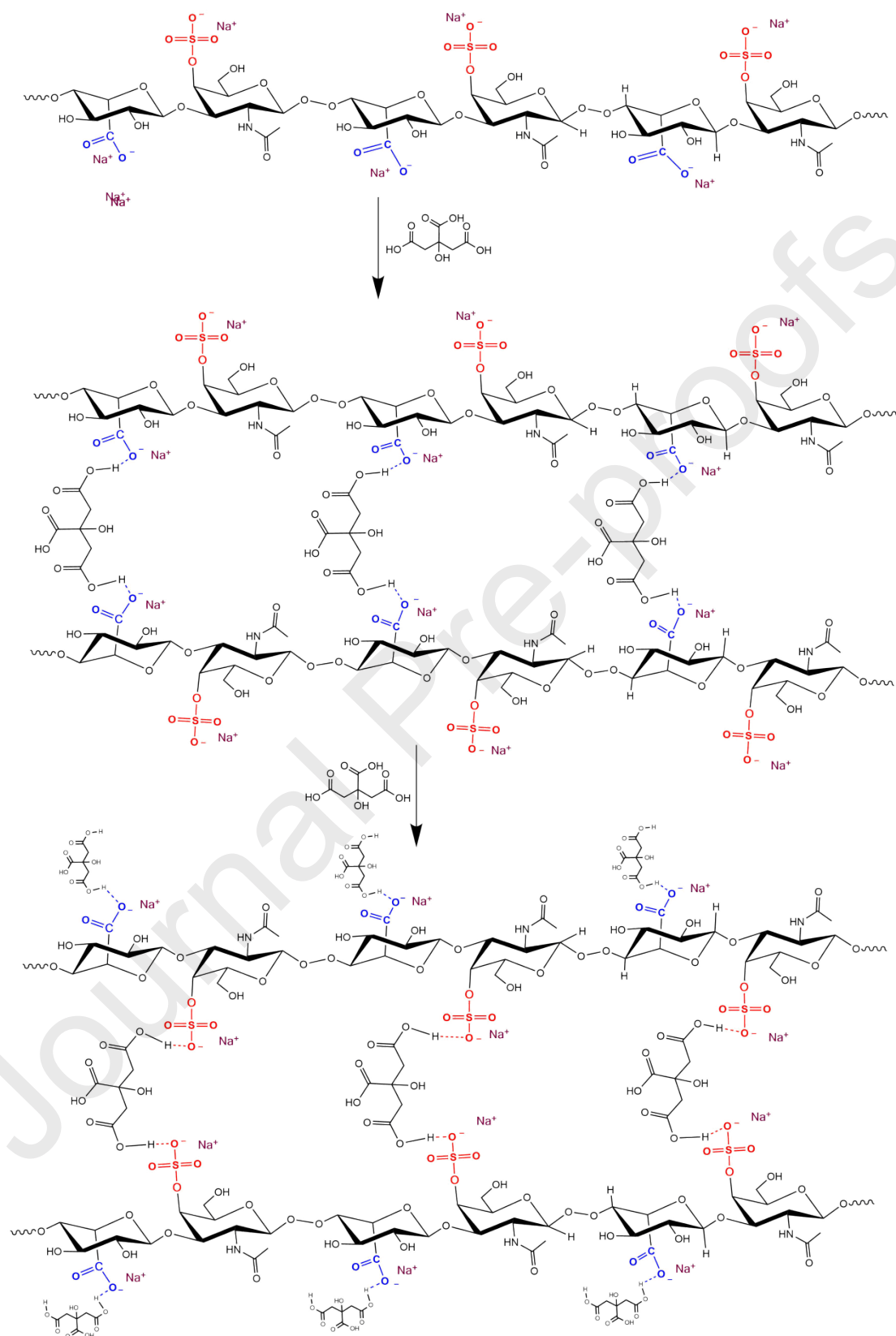


Figure S11. Tentative cross-linking reaction scheme of CA with CSA.

Morphological Studies, Thermal Behavior and Proton Conductivity for CA:CSA(X) Electrolytes with $X > 82.3$

Powders were obtained for $X > 82.3$.

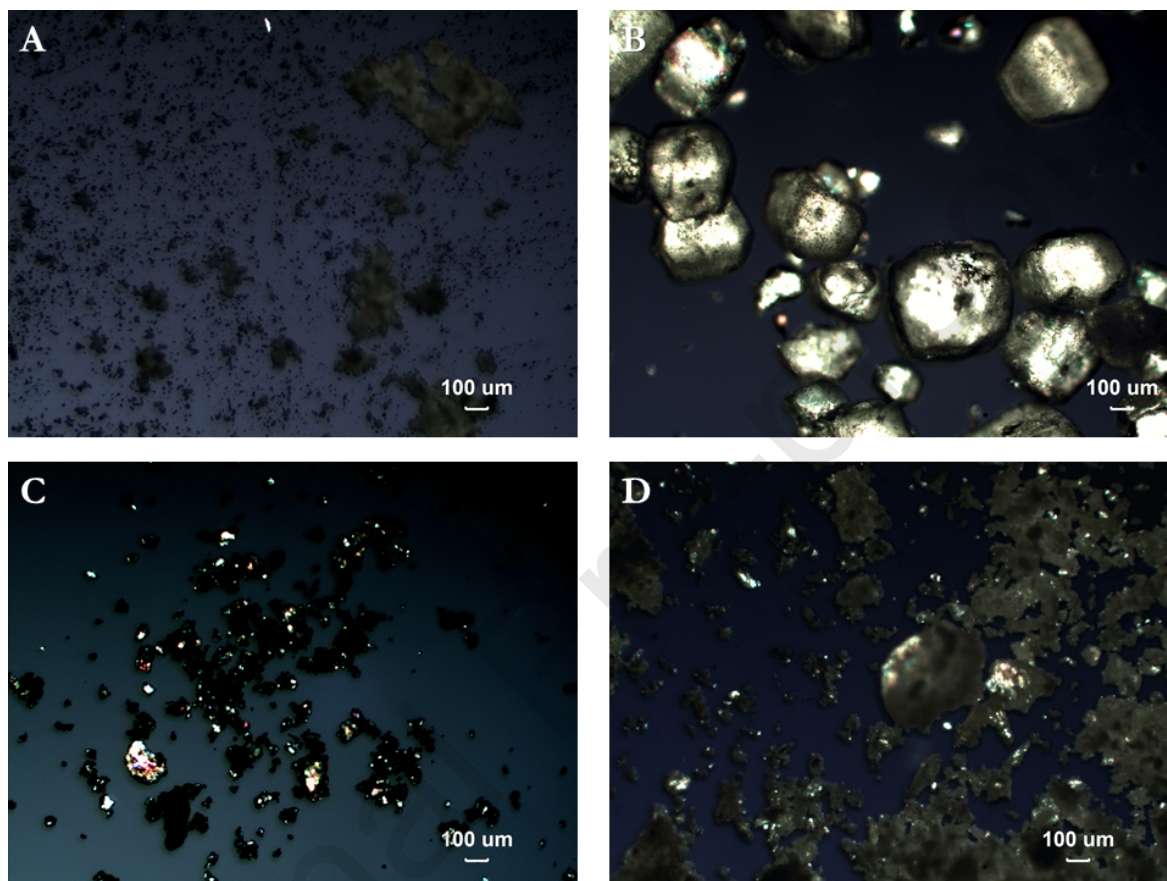


Figure S12. POM images of (A) CSA; (B) CA and CA:CSA(X) electrolytes with $X = 92.5$ (C) and 86.1 (D)

The POM images obtained for the electrolytes (Figures S12C and S12D) show that the samples are heterogeneous and semi-crystalline (Figures S12C and S12D). Comparison with the POM images of the precursors (Figures S12A and S12B) demonstrates that the amorphous phase is due to the CSA moiety, while the birefringent regions are due to CA.

The thermal data obtained for the same set of samples is presented in Figure S13.

The TGA curves obtained for CSA, CA and the CA:CSA(X) electrolytes with $X > 82.3$ are represented in Figure S13. The onset decomposition temperatures for CSA and CA are 233 and 179 °C, respectively. Both these values are in perfect agreement with those reported in the literature for

CSA [11,14], and CA [15,16]. In all cases, the adsorbed water was lost at temperatures below 120 °C (Table 1). With the exception of the sample with $X = 86.1$, which contains *ca.* 4.5%(w/w) of water, the electrolytes contain between 6-8 %(w/w) of water and CSA, 11%(w/w) of water. The onset of degradation of all the CA:CSA samples occurred at 120-140 °C, regardless of the CA:CSA mass ratio. Figure S13 points out a decrease of the thermal stability of the materials resulting from the combination of CSA and CA when compared to CA and other analog systems [11,14,17,18].

These results point out that the thermal stability of the powders is in line with that of the CA:CSA(X) samples with $X < 82.3$

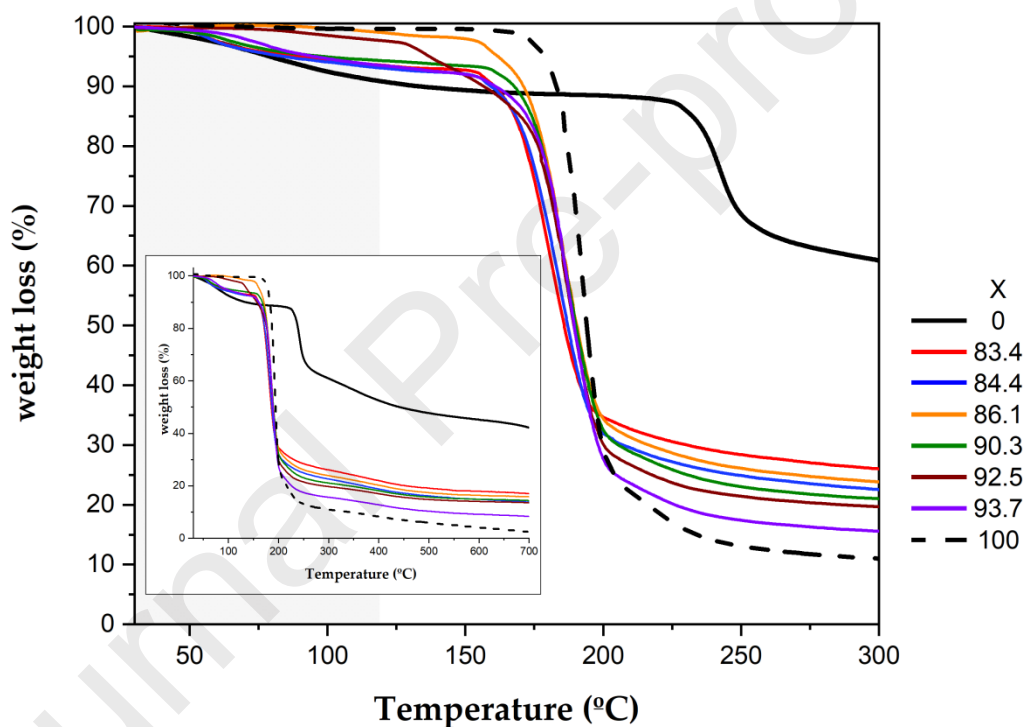


Figure S13. TGA curves for CSA, CA and CA:CSA(X), with $X > 82.3$.

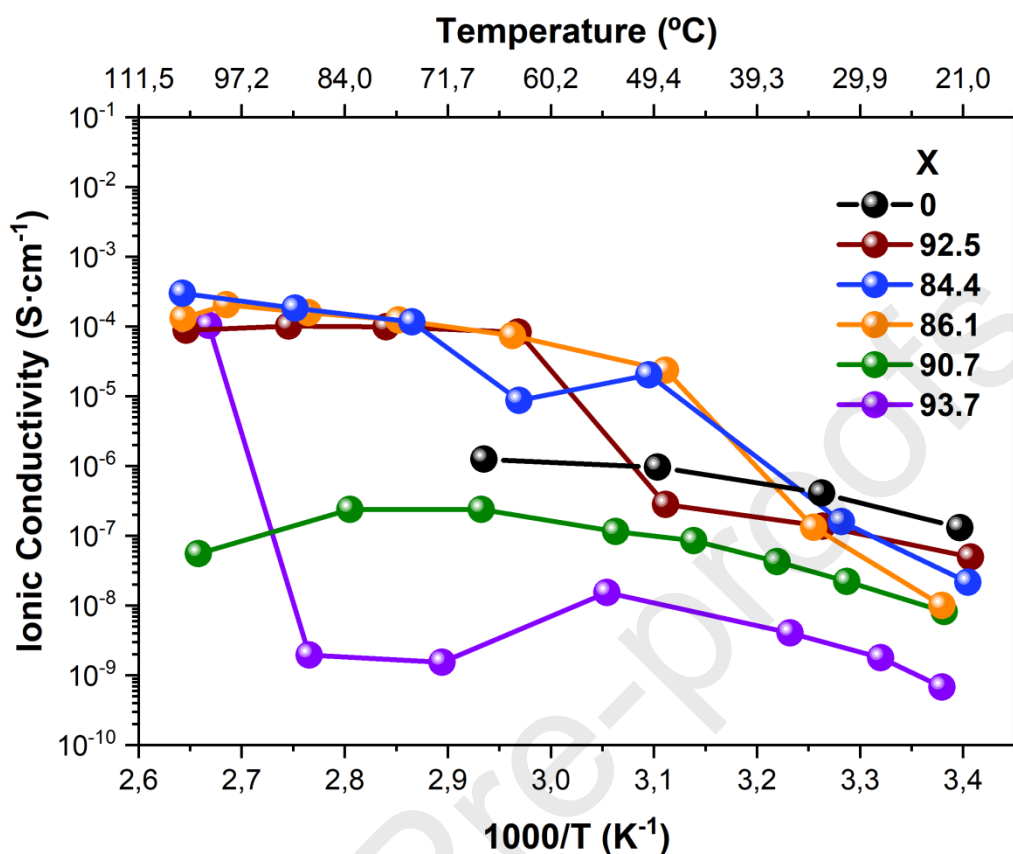


Figure S14. Arrhenius conductivity plots for CSA and CA:CSA(X), with $X > 82.3$.

The Arrhenius conductivity data collected for CSA and the samples with $X \geq 82.3$ are shown in Figure S14. CSA exhibits ionic conductivity values between $1.3 \times 10^{-7} \text{ S cm}^{-1}$ and $1.2 \times 10^{-6} \text{ S cm}^{-1}$ over the range of 20-70 °C. Addition of a high amount of CA to the CSA solution systematically led to the formation of materials with lower ionic conductivity when compared with the CSA precursor. As reported in Section 3.2, these samples feature a high CA content, which leads to a) to a higher acidification of the CSA solution ($\text{pH} < 2.0$), thus promoting a series of structural changes in the polysaccharide structure that resulted in both a more compact conformation [9,11–13,19] and a strengthening of the bonds to the Na^+ cations [20,21], and b) the formation of materials with higher crystallinity. Both factors are known to reduce ion mobility due to loss of mobility of the polymeric chains.

A small temperature increase (up to 40-60 °C) resulted, in all cases, in an increase in ionic conductivity. However, with further increases of temperature, the samples with $X > 82.3$ started to

experience loss of hydration waters and specific microscopical changes – as evidenced by TGA analysis – which led to variations in the proton conductivity. Even so, samples with $X = 86.1$ and 92.5 achieved conductivity values higher than 10^{-4} Scm^{-1} at temperatures as low as $70 \text{ }^\circ\text{C}$, making them interesting for electrochemical applications.

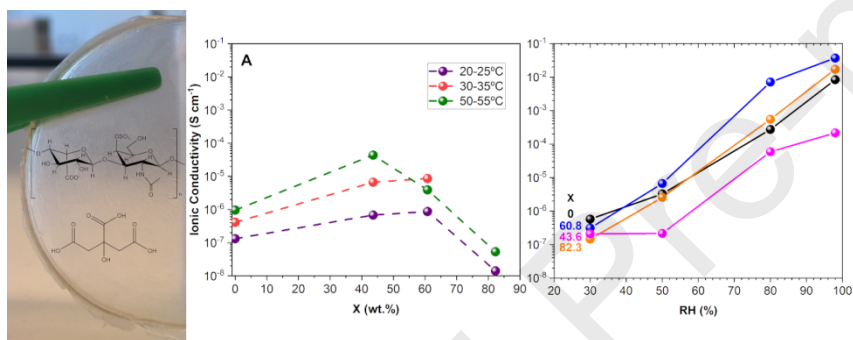
References:

1. Hamer, G.K.; Perlin, A.S. A ^{13}C -N.M.R. spectral study of chondroitin sulfates A, B, and C: evidence of heterogeneity. *Carbohydr. Res.* 1976, 49, 37–48.
2. Bociek, S.M.; Darke, A.H.; Welti, D.; Rees, D.A. The ^{13}C -NMR spectra of hyaluronate and chondroitin sulphates: further evidence on an alkali-induced conformation change. *Eur. J. Biochem.* 1980, 109, 447–456.
3. Scheidt, H.A.; Schibur, S.; Magalhães, A.; de Azevedo, E.R.; Bonagamba, T.J.; Pascui, O.; Schulz, R.; Reichert, D.; Huster, D. The mobility of chondroitin sulfate in articular and artificial cartilage characterized by ^{13}C magic-angle spinning nmr spectroscopy. *Biopolymers* 2010, 93, 520–532.
4. Schiller, J.; Naji, L.; Huster, D.; Kaufmann, J.; Arnold, K. ^1H and ^{13}C HR-MAS NMR investigations on native and enzymatically digested bovine nasal cartilage. *MAGMA* 2001, 8661, 37–41.
5. Fischer, J.W.; Merwin, L.H.; Nissan, R.A. NMR investigation of the thermolysis of citric acid. *Appl. Spectrosc.* 1995, 49, 120–126.
6. Kakihana, M.; Arima, M.; Nakamura, Y.; Yashima, M.; Yoshimura, M. Spectroscopic characterization of precursors used in the pechini-type polymerizable complex processing of barium titanate. *Chem. Mater.* 1999, 11, 438–450.
7. Y. Zhao, Z. Jiang, L. Xiao, T. Xu, S. Qiao, H. Wu, Chitosan membranes filled with biomimetic mineralized hydroxyapatite for enhanced proton conductivity, *Solid State Ionics.* 187 (2011) 33–38. doi:10.1016/j.ssi.2011.01.019.
8. J.F. Piai, L.C. Lopes, A.R. Fajardo, A.F. Rubira, E.C. Muniz, Kinetic study of Chondroitin sulphate release from chondroitin sulphate/chitosan complex hydrogel, *J. Mol. Liq.* 156 (2010) 28–32. doi:10.1016/j.molliq.2010.05.017.
9. J.F. Piai, A.F. Rubira, E.C. Muniz, Self-assembly of a swollen chitosan/chondroitin sulfate hydrogel by outward diffusion of the chondroitin sulfate chains, *Acta Biomater.* 5 (2009) 2601–2609. doi:10.1016/j.actbio.2009.03.035.
10. A.R. Fajardo, M.B. Silva, L.C. Lopes, J.F. Piai, A.F. Rubira, E.C. Muniz, Hydrogel based on an alginate- Ca^{2+} /chondroitin sulfate matrix as a potential colon-specific drug delivery system, *RSC Adv.* 2 (2012) 11095–11103. doi:10.1039/c2ra20785k.
11. A.R. Fajardo, J.F. Piai, A.F. Rubira, E.C. Muniz, Time- and pH-dependent self-rearrangement of a swollen polymer network based on polyelectrolytes complexes of chitosan/chondroitin sulfate, *Carbohydr. Polym.* 80 (2010) 934–943. doi:10.1016/j.carbpol.2010.01.009.
12. A.R. Fajardo, L.C. Lopes, A.J.M. Valente, A.F. Rubira, E.C. Muniz, Effect of stoichiometry and pH on the structure and properties of chitosan/chondroitin sulfate complexes, *Colloid Polym. Sci.* 289 (2011) 1739–1748. doi:10.1007/s00396-011-2497-6.

13. M. Bathe, G.C. Rutledge, A.J. Grodzinsky, B. Tidor, A coarse-grained molecular model for glycosaminoglycans: application to chondroitin, chondroitin sulfate, and hyaluronic acid, *Biophys. J.* 88 (2005) 3870–3887. doi:10.1529/biophysj.104.058800.
14. Fajardo, A.R.; Lopes, L.C.; Pereira, A.G.B.; Rubira, A.F.; Muniz, E.C. Polyelectrolyte complexes based on pectin-NH₂ and chondroitin sulfate. *Carbohydr. Polym.* 2012, 87, 1950–1955.
15. Barbooti, M.M.; Al-Sammerrai, D.B. Thermal decomposition of citric acid. *Thermochim. Acta* 1986, 98, 119–126.
16. Wyrzykowski, D.; Hebanowska, E.; Nowak-Wiczek, G.; Makowski, M.; Chmurzyński, L. Thermal behaviour of citric acid and isomeric aconitic acids. *J. Therm. Anal. Calorim.* 2011, 104, 731–735.
17. Denuzière, A.; Ferrier, D.; Domard, A.; Ferrief, D.; Domard, A. Chitosan-chondroitin sulfate and chitosan-hyaluronate polyelectrolyte complexes. Physico-chemical aspects. *Carbohydr. Polym.* 1996, 29, 317–323.
18. Wang, L.F.; Shen, S.S.; Lu, S.C. Synthesis and characterization of chondroitin sulfate-methacrylate hydrogels. *Carbohydr. Polym.* 2003, 52, 389–396.
19. Tripathi, B.P.; Shahi, V.K. Functionalized organic-inorganic nanostructured N-p-carboxy benzyl chitosan– silica–PVA hybrid polyelectrolyte complex as proton Exchange Membrane for DMFC applications. *J. Phys. Chem. B* 2008, 112, 15678–15690.
20. Balme, S.; Rixte, J.; Boustta, M.; Vert, M.; Henn, F. Complex impedance spectroscopy to investigate degradable chondroitin–poly(amino-serinate) complexes. *Polym. Degrad. Stab.* 2013, 98, 2161–2167.
21. Chakrabarti, B.; Park, J.W.; Stevens, E.S. Glycosaminoglycans: structure and interaction. *CRC Crit. Rev. Biochem.* 1980, 8, 225–313.

Highlights

- The combination of Chondroitin sulfate (CSA) and citric acid (CA) led to the preparation of self-standing electrolyte films with improved mechanical properties.
- CA acts as proton donor, and cross-linker, able to influence samples morphology
- CA:CSA material feature a high ionic conductivity that makes it interesting for applications in solid state chemistry



Author Contributions:

The manuscript was written with contributions from all authors. All authors have given approval to the final version of the manuscript.

Filipe M. Santos: Conceptualization, Investigation, Formal analysis, Writing – Original Draft, Writing – Review & Editing

Paula C. Barbosa: Investigation, Formal analysis, Writing – Original Draft, Writing – Review & Editing;

Rui F. P. Pereira: Investigation, Formal analysis, Writing – Original Draft, Writing – Review & Editing;

M. M. Silva: Supervision; Validation; Writing – Original Draft, Writing – Review & Editing

Helena M.R. Gonçalves: Investigation, Formal analysis, Writing – Original Draft, Writing – Review & Editing;

Sílvia C. Nunes: Investigation, Formal analysis, Writing – Original Draft, Writing – Review & Editing

Filipe Figueiredo: Visualization, Formal analysis, Supervision, Writing – Original Draft, Writing – Review & Editing; Project administration

Artur J. M. Valente: Investigation, Formal analysis; Validation; Writing – Original Draft; Writing . Review & Editing;

Verónica de Zea Bermudez: Visualization; Conceptualization; Supervision; Writing – Original Draft; Writing – Review & Editing; Project administration.

Declaration of interests

The authors declare that they have no known competing financial interests or personal relationships that could have appeared to influence the work reported in this paper.

The authors declare the following financial interests/personal relationships which may be considered as potential competing interests: